Chapter 13 | Stratified Atmospheric Boundary Layers

13.1 Types of Atmospheric Boundary Layers

Atmospheric boundary layers are usually classified into different types, depending on the atmospheric stability and the dominating mechanism of turbulence generation in the boundary layer. Turbulence is moderately strong and more or less continuous throughout the PBL under very windy and near-neutral stability conditions. It is essentially generated by surface friction and wind shear and, hence, is referred to as shear-generated or mechanical turbulence. The resulting near-neutral PBL has already been described in Chapter 10.

Vigorous turbulence can also be generated by convection over a heated surface and is generally referred to as convective turbulence. More often, over a heated surface, both the shear and convective mechanisms of turbulence generation operate simultaneously, especially in the surface layer. Wind shear is strongest near the surface and its influence is largely confined to the surface layer. Convective turbulence dominates in the overlying, deep mixed layer, while much weaker shear-generated turbulence occurs in the transition layer near the top of the PBL. Such a PBL is generally referred to as the convective boundary layer (CBL) whose three-layer structure is schematically shown in Figure 13.1.

The surface layer constitutes the lowest 5–10% of the CBL in which significant variations (gradients) of wind speed, potential temperature and specific humidity with height are observed to occur, but mean wind direction remains nearly constant with height. Immediately above the shallow surface layer lies the much deeper mixed layer, which extends almost up to the base of the capping inversion. It is characterized by a uniform potential or virtual potential temperature and nearly uniform winds and specific humidity. The mixed-layer depth or the height of inversion base z_i constitutes the most important height or length scale in the mixed-layer similarity theory. The mixed layer is capped by a stabley stratified transition layer in which turbulence is suppressed with increasing height and completely vanishes at the top of the PBL. The transition layer is characterized by intermittently penetrating thermals from below and entrainment of the nonturbulent free-atmospheric

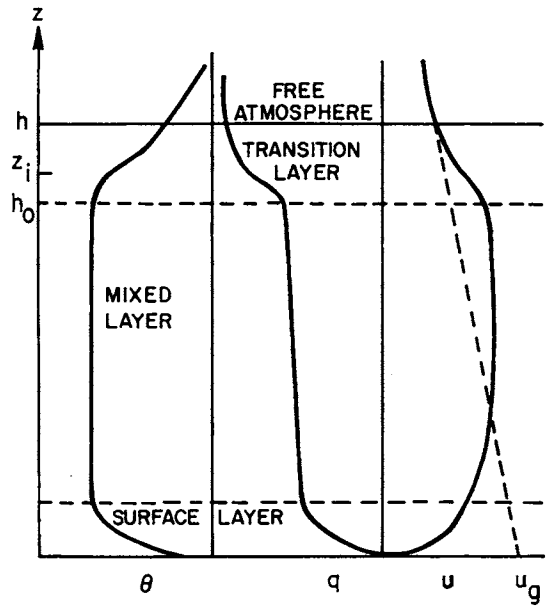

Figure 13.1 Schematic of the vertical distributions of mean potential temperature (Θ), specific humidity (Q), wind speed (U), and geostrophic wind (U_g), showing the three-layer structure of the convective boundary layer.

warmer and drier air from above, particularly during the late morning period of rapidly growing PBL. The transition layer typically extends from $0.9z_i$ to $1.2z_i$, although both the lower and upper boundaries can vary over a wider range.

In contrast to the CBL, the atmospheric boundary layer over a cold surface (e.g., any land surface during a clear night) is called the stable boundary layer (SBL), because it is stably stratified due to increasing temperature or potential temperature with height (also referred to as an inversion condition). Turbulence in the SBL is essentially shear generated, but is much weakened and sometimes entirely suppressed in the upper part by the action of buoyancy. Above the shallow surface layer, turbulence in the SBL is highly intermittent (episodic), patchy, and frequently mixed with internal gravity waves. In terms of the boundary layer height or thickness (h), the SBL is much thinner (typically, $h \cong 100$ m) than the CBL (typically, $h \cong 1000$ m).

The atmospheric boundary layer during the transitional near-neutral stability regime between unstable and stable conditions is also called the near-neutral boundary layer (NNBL). The surface is either slightly warmer or cooler than the air above. The morning and evening transition periods, when the sensible heat exchange between the surface and the atmosphere vanishes momentarily, as it changes sign from negative (downward flux) to positive (upward flux) and vice

versa, are often marked by rapid changes in the PBL height, mean winds, and turbulence. Thus, the transitional NNBL is rapidly evolving under changing surface energy fluxes and is essentially nonstationary. It is the least studied and the least understood of all the atmospheric boundary layers.

The above classification of the PBL according to three broad stability regimes is somewhat artificial and for convenience only. More specific and quantitative PBL stability parameters, such as the bulk Richardson number and the ratio h/L of the PBL height to the Obukhov length, are found to vary continuously over wide ranges. One of these can be used to represent more systematically the important effects of stability on the mean flow and turbulence structure of the PBL as it varies from extremely unstable or convective to extremely stable conditions in the atmosphere. Still, in describing the typical observed structure of the PBL under convective, near-neutral and stable conditions, we often use the broader, qualitative stability characterizations and also the corresponding designations of the atmospheric boundary layer as CBL, NNBL and SBL. Since most of the PBL theories and models are more generic in their formulation and concepts, however, these will be reviewed without regard to the PBL stability. But, their lack of validity and other limitations under certain stability conditions will be discussed. In describing the PBL theories and models, it is also important to specify the presence or lack of certain simplifying conditions, such as stationarity and horizontal homogeneity of the PBL.

13.1.1 Horizontally homogeneous PBL

The atmospheric boundary layer formed under and driven by large-scale flows (e.g., geostrophic or gradient winds) over a reasonably flat and uniform surface can essentially be considered horizontally homogeneous, especially over horizontal dimensions of up to 100 km, i.e., smaller than the typical resolution of the synoptic observing network. Such an idealized PBL may evolve gradually with time in response to the similar evolution of the large-scale flow with time. Even when the large-scale flow is steady over several days, the PBL evolves diurnally as a result of the diurnal heating and cooling of the surface. Diurnal changes in the PBL are observed to become small and, sometimes, even insignificant over open ocean and sea surfaces and also extensive snow- and ice-covered surfaces over the polar regions during winter. Over a short period of the order of an hour, however, even a diurnally evolving PBL over a bare and dry land surface can be considered to be quasi-stationary when one considers its short-term averaged properties. This idealized (horizontally homogeneous and quasi-stationary) PBL has been the focus of many experiments as well as simpler theories and models that will be discussed in more detail in later sections.

The PBL depth or mixing height is the most important length scale which determines the size of the largest energy-containing eddies, average wind speed and direction shears in the PBL, as well as the overall stability of the PBL. The PBL depth shows strong diurnal variations in response to the diurnal heating and cooling of the surface. It increases throughout the day, becomes maximum (typically, 1 km) in the late afternoon, and then rapidly collapses to its typical nighttime value of the order of 100 m. At night, mixing height rarely stays constant, but usually oscillates around its mean value in response to periodic turbulence generation episodes. The maximum mixing height during the afternoon also shows large seasonal and spatial variations as shown in Figure 13.2 for the continental United States (Holzworth, 1964).

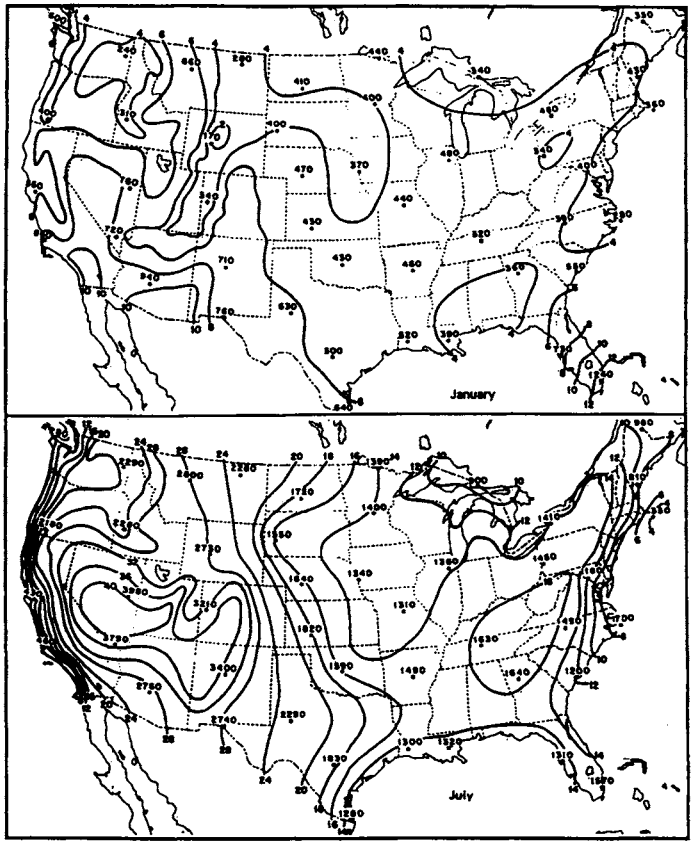

Figure 13.2 Spatial variation of mean maximum mixing height in meters over the continental United States for the months of (a) January and (b) July. [From Holzworth (1964).]

13.1.2 Nonhomogeneous boundary layers

The idealized horizontally homogeneous PBL may be expected to develop over extensive flat and uniform water surfaces, such as open seas, oceans and large lakes, as well as over a variety of land surfaces, such as deserts, grasslands, and forests, covering more than 80% of the earth's surface. However, over most of the developed land areas, which are marked by residential, industrial, commercial, agricultural, and recreational use, the atmospheric boundary layer is nonhomogeneous and frequently in a state of transition from one land use type to another. Surface inhomogeneities affecting the PBL flow include boundaries between land and water surfaces (coastlines); urban and rural areas (urban heat and roughness islands); different types of vegetation; and hills and valleys. In going over these land use and terrain inhomogeneities, the PBL flow encounters sudden or gradual changes in surface roughness, temperature, wetness, or elevation. Quite often, changes in several surface properties occur simultaneously. The mesoscale atmospheric circulation systems, such as land-sea breezes, urban heat island, mountain and valley winds, and others associated with complex topography, are likely to have nonhomogeneous boundary layers in them. Some of the cases of nonhomogeneous atmospheric boundary layers will be covered in more detail in Chapter 14.

13.2 Similarity Theories of the PBL

The observed mean wind, temperature and specific humidity profiles in the homogeneous atmospheric boundary layer, such as those presented earlier in Chapters 5 and 6, as well as turbulence structure (e.g., variances and covariances) are best represented in an appropriate similarity theory framework. A similarity theory, based on dimensional analysis, provides the most appropriate scales for normalizing variables into dimensionless groups or similarity parameters, organizing and presenting experimental data in the most efficient manner, and empirically deriving the various similarity relations or predictions. Most generalized parameterizations of the PBL including drag and heat transfer relations are also based on some form of similarity scaling. The surface layer similarity theories and scaling have already been reviewed and discussed in Chapters 9–12. Chapter 10 also covers the simpler case of the neutral PBL whose depth is not restricted by any low-level inversion. In this section, we will review the similarity theories and scaling for the more frequently encountered stratified atmospheric boundary layers including the CBL and the SBL.

13.2.1 Mixed-layer similarity theory/scaling

In unstable and convective PBLs, there is a mixed layer above the surface layer in which the mean potential temperature is observed to be nearly uniform (Stull, 1988; Garratt, 1992; Kaimal and Finnigan, 1994). Variations in specific humidity and mean velocity are also observed to be small over the depth of the mixed layer. Figure 13.3 shows such a convective mixed layer within the marine boundary layer whose depth (h) can be identified from mean potential temperature and specific humidity profiles.

Deardorff (1970b) proposed a similarity hypothesis that turbulence structure in the convective mixed layer depends only on the virtual heat flux $H_{v0}/\rho c_p$, the buoyancy variable g/T_{v0}, the height above the surface z, and the height z_i of the base of inversion which caps the mixed layer. The appropriate scaling parameters for the mixed-layer similarity are z_i and the convective velocity

$$W_* = \left(\frac{g}{T_{v0}} \frac{H_{v0}}{\rho c_p} z_i\right)^{1/3} \tag{13.1}$$

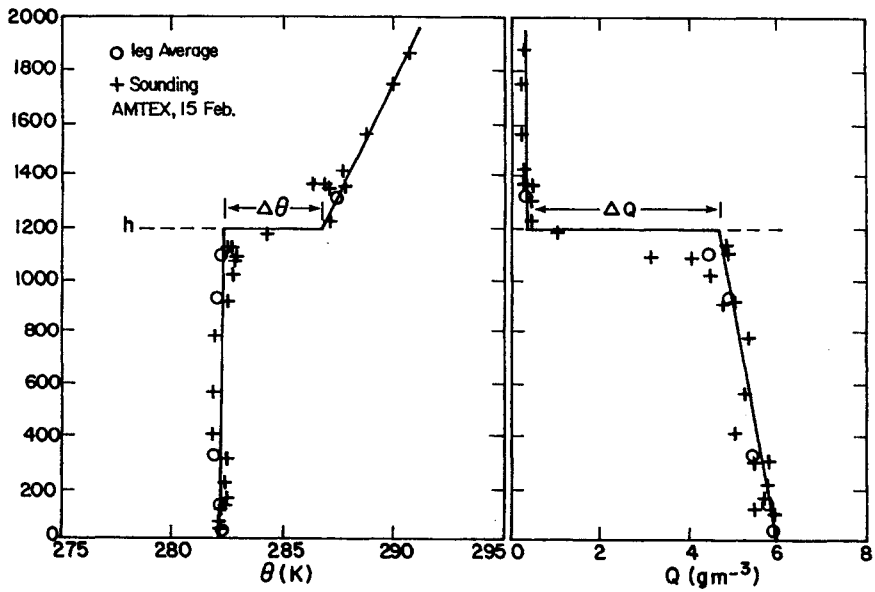

Figure 13.3 Observed mean potential temperature (θ) and specific humidity (Q) profiles under convective conditions on February 15, 1975, during AMTEX. [After Wyngaard *et al.* (1978).]

The mixed-layer similarity theory predicts that σ_u/W_*, σ_v/W_*, etc., and other appropriately scaled turbulence statistics must be unique functions of z/z_i only. This is strictly valid only within the mixed layer ($0.1z_i < z \leq z_i$) of the CBL with $-z_i/L > 10$. Actual observations of turbulence in the CBL (Figure 13.4), however, indicate that there is hardly any dependence of σ_u/W_* and σ_v/W_* on z/z_i and, for all practical purposes,

$$\sigma_u/W_* \cong \sigma_v/W_* \cong 0.60 \tag{13.2}$$

The standard deviation of vertical velocity fluctuations in the CBL has been observed to show a much stronger dependence on z/z_i (see Figure 13.4). It increases with height, attains a broad maximum in the middle of the mixed layer, and decreases again in the upper part of the CBL (Caughey and Palmer, 1979; Sorbjan, 1989). For most practical applications, $\sigma_w/W_* \cong 0.60$ represents an average value for the whole mixed layer; more detailed empirical expressions of the same in different layers are given by Hanna (1982).

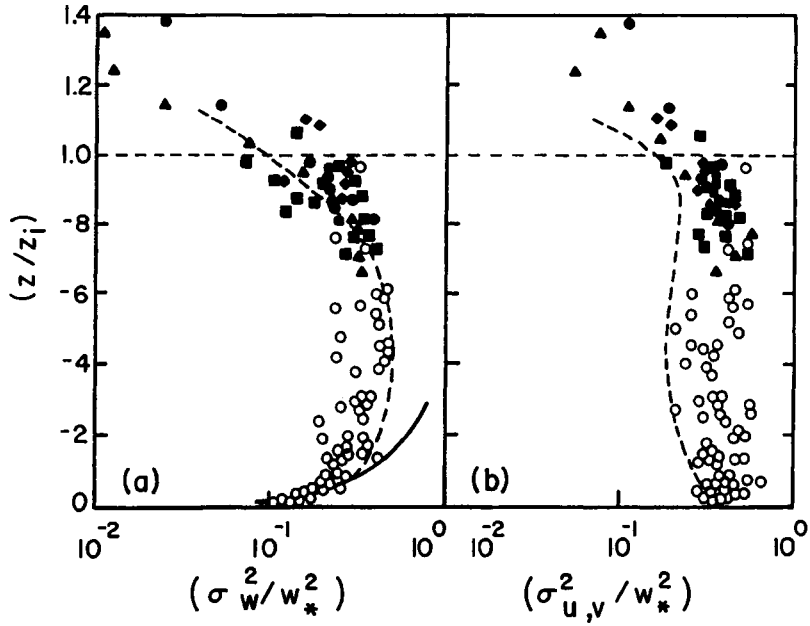

Figure 13.4 Normalized variances of (a) vertical and (b) horizontal velocity fluctuations as functions of z/z_i. Solid line represents the local free convection prediction and dashed lines represent the convection tank results of Willis and Deardorff (1974). [From Caughey and Palmer (1979).]

Combining the mixed-layer similarity relations for σ_u, σ_v and σ_w into the definition of TKE, one obtains

$$E = 0.36W_*^2 + 0.9\left(\frac{z}{z_i}\right)^{2/3}\left(1 - 0.8\frac{z}{z_i}\right)^2 W_*^2 \tag{13.3}$$

Alternatively, for most practical purposes,

$$E \cong 0.54W_*^2 \tag{13.4}$$

may represent the layer-averaged value of the TKE in the convective mixed layer. An empirical expression for rate of energy dissipation in the same is:

$$\varepsilon = \frac{W_*^3}{z_i}\left(0.8 - 0.3\frac{z}{z_i}\right) \tag{13.5}$$

which yields the layer-averaged value of $0.5W_*^3/z_i$.

Higher moments of turbulence in the mixed layer are also found to be scaled by W_*. In particular, the normalized third moment of vertical velocity $\overline{w^3}/W_*^3$, or skewness $S = \overline{w^3}/\sigma_w^3$, is observed to be significantly positive, indicating much larger positive velocities in convective updrafts compared to the average negative velocity in downdrafts. Since the average vertical velocity is essentially zero in a horizontally homogeneous CBL, the horizontal area occupied by downdrafts is much (about 50%) larger than that occupied by updrafts. This is also confirmed by estimated probability density functions of vertical velocity in the CBL (Arya, 1999, Chapter 5).

The mixed-layer similarity scaling may not be valid in the transition layer above the inversion base. Turbulence and diffusion processes in this layer are also influenced by entrainment of free atmospheric air, stronger wind speed and direction shears, and potential temperature gradients observed in the transition layer (Stull, 1988).

13.2.2 Rossby-number similarity theory

The Rossby-number similarity theory for the stratified PBL is based on a similarity hypothesis proposed by Kazanski and Monin (1961) that the PBL structure is determined by all the variables that were included in the M–O similarity hypothesis plus the Coriolis parameter f. The latter yields an addition length scale $u_*/|f|$ which is a measure of the height of the neutral PBL

($h \cong 0.25u_*/|f|$). The normalized height of the stratified PBL is predicted to be a unique function of the stability parameter, i.e.,

$$h|f|/u_* = F_h(\mu_*) \tag{13.6}$$

where $\mu_* = u_*|f|/L$ is the relevant stability parameter. The similarity theory also predicts that in a barotropic PBL, the dimensionless ageostrophic wind components $(U - U_g)/u_*$ and $(V - V_g)/u_*$, as well as turbulence statistics, must be unique functions of the dimensionless height, $z|f|/u_*$, and μ_* only. An appropriate matching of the PBL similarity profiles with those of the surface layer also yields geostrophic drag or resistance laws (Arya, 1975; Zilitinkevich *et al.*, 1976) which can be used for parameterizing the PBL in large-scale atmospheric circulation models. These resistance laws contain the surface Rossby number, $G|f|/z_0$, as an important parameter, which explains the name given to this similarity theory and scaling.

Tennekes (1982) has given a formal and elegant derivation of the velocity-defect profile relations (10.11) and the geostrophic drag relations (10.20) for the barotropic, neutral PBL. The proposed extensions of the same relations consider the dependence of the various similarity functions, including A, B, etc., on the stability parameter μ_* (Clarke and Hess, 1974; Arya, 1975). This also implies that the dimensionless PBL height must also be a unique function of μ_* as in Equation (13.6). However, Deardorff (1972a, b, 1974) and others have pointed out that it was not true under unstable and convective conditions in which the PBL height is not at all related to u_*/f or μ_*, but is determined by the height of the lowest inversion base. For this reason, the Rossby-number similarity scaling cannot be valid under unstable and convective conditions. Its validity in the stable boundary layer (SBL) is also somewhat limited to slightly and moderately stable conditions during which there is continuous exchange between adjacent layers in the vertical, i.e., turbulence is continuous throughout the SBL. Under very stable conditions, turbulence becomes highly intermittent and sporadic, so that upper layers may become decoupled from the surface layer. Any similarity scaling based on the surface fluxes will not be appropriate.

For the SBL with more or less continuous turbulence, Zilitinkevich (1972) derived the following diagnostic relationship for steady state or stationary conditions:

$$h = d(u_*L/|f|)^{1/2} \tag{13.7}$$

in which d is an empirical constant. The above relationship implies a simple form of the similarity function in Equation (13.6) as

$$h|f|/u_* = d\mu_*^{-1/2} \tag{13.8}$$

These SBL height relations have been tested against experimental data obtained at several flat and approximately homogeneous sites (Garratt, 1982). The estimated values of d range from 0.2 to 0.7 with an average value of about 0.4 which is also the value suggested by numerical modeling studies (Brost and Wyngaard, 1978). It has been shown that d may depend on the time after transition, surface cooling rate, terrain slope and possibly other factors.

The above diagnostic similarity relation may not be valid for an evolving SBL for several hours after the transition time. Prognostic equations for the SBL height have been proposed for such an evolving boundary layer (Stull, 1988, Chapter 12). The SBL evolves rather slowly in time and rarely reaches a steady or equilibrium state. This may explain why correlations between the observed and theoretically predicted SBL heights are not usually very strong (Arya, 1981; Koracin and Berkowicz, 1988).

The mean velocity profiles in the similarity form are usually expressed as

$$\begin{aligned}(U - U_g)/u_* &= F_u(fz/u_*, \mu_*) \\ (V - V_g)/u_* &= F_v(fz/u_*, \mu_*)\end{aligned} \tag{13.9}$$

The corresponding geostrophic drag relations are

$$\begin{aligned}U_g/u_* &= \frac{1}{k}[\ln(u_*/fz_0) - A(\mu_*)] \\ V_g/u_* &= -B(\mu_*)/k\end{aligned} \tag{13.10}$$

Geostrophic drag and heat transfer relations in the SBL have been extensively studied and the similarity functions $A(\mu_*)$, $B(\mu_*)$, etc., have been evaluated from experimental data as well as numerical models of the SBL (Arya, 1975, 1977, 1984). Experimental estimates of the same show large scatter, reflecting possible effects of baroclinicity and other factors (Sorbjan, 1989; Garratt, 1992).

13.2.3 Generalized similarity theory

Recognizing the importance of the PBL height (h) as an independent height scale and the lack of general validity of Equation (13.6), Deardorff (1972a) utilized z/h and h/L as the dimensionless height and stability parameters. Zilitinkevich and Deardorff (1974) also proposed that $u_*/|f|$ be replaced by h in the PBL similarity formulation for the entire range of stability conditions. It was later recognized, however, that $u_*/|f|$ cannot be ignored entirely, and $h|f|/u_*$ should also be considered as an additional parameter in any generalized similarity theory. Further consideration of baroclinicity added two more

similarity parameters to the expanding list of the same (Arya and Wyngaard, 1975). Subsequently, the similarity functions A, B, etc., have been evaluated as functions of h/L (Yamada, 1976). These are also characterized by large scatter, possibly due to baroclinicity and other parameters. The relations involving layer-averaged (over the PBL depth) winds, temperature, etc., are found to be less sensitive to the effects of baroclinicity (Arya, 1978; Garratt *et al.*, 1982). For example, the layer-averaged wind speed in an unstable PBL is given by

$$V_m/u_* = \frac{1}{k}\left[\ln\frac{h}{z_0} - 0.5\ln|h/L| - 2.3\right] \tag{13.11}$$

For representing the turbulence structure of unstable and convective boundary layers, it is much simpler to use the mixed-layer similarity scaling than the generalized similarity scaling discussed above. Therefore, most turbulence and diffusion data in the CBL are presented using the mixed-layer scaling.

Turbulence data in slightly and moderately stable boundary layers with more or less continuous turbulence are best represented in the generalized similarity framework, i.e., as functions of z/h and h/L. The parameter $h|f|/u_*$ appears to be uniquely related to h/L and may not be an independent parameter affecting turbulence structure. Even the influence of the stability parameter does not appear to be overly significant, when normalized turbulence statistics are represented as functions of z/h. For example, in a steady PBL over a flat terrain, the vertical profiles of TKE and fluxes can be represented as (Lenschow *et al.*, 1988; Smedman, 1991; Rao and Nappo, 1998):

$$E \cong 5.75u_*^2\left(1 - \frac{z}{h}\right)^{\alpha_1} \tag{13.12}$$

$$\tau = \rho u_*^2\left(1 - \frac{z}{h}\right)^{\alpha_1} \tag{13.13}$$

$$H = H_0\left(1 - \frac{z}{h}\right)^{\alpha_2} \tag{13.14}$$

in which the values of exponents α_1 and α_2 may depend on the temporal development or evolution of the SBL, terrain slope, and other factors. For a well developed or steady SBL, $\alpha_1 \cong 1.75$ and $\alpha_2 \cong 1.5$ (Lenschow *et al.*, 1988; Smedman, 1991). Equations (13.12)–(13.14) may be considered as extensions of the surface-layer similarity relations to the whole SBL.

13.2.4 Local similarity theory/scaling

For the stable boundary layer, Nieuwstadt (1984) proposed a local similarity hypothesis that, above the surface layer, mean gradients and turbulence statistics in the SBL follow a local similarity scaling based on the local (not surface) fluxes. Thus, analogous to the Monin–Obukhov similarity scales, the local scaling parameters are defined as

$$u_{*\ell} = (\tau/\rho)^{1/2};\ \theta_{*\ell} = -H/\rho c_p u_{*\ell}$$
$$\Lambda = T_v u_{*\ell}^2/kg\theta_{*\ell} \tag{13.15}$$

where $u_{*\ell}$ and $\theta_{*\ell}$ are the local friction velocity and temperature scale respectively, and Λ is a local buoyancy length scale which is analogous to the Obukhov length in the surface layer.

The local similarity theory predicts that appropriately scaled (normalized) mean velocity and temperature gradients, as well as turbulence statistics, at any height in the SBL must be some universal functions of the local stability parameter z/Λ. Furthermore, under very stable conditions when upper layers become decoupled from the surface layer and even from adjacent layers, and turbulence is sporadic and becomes independent of z, i.e., under the so-called z-less stratification (Monin and Yaglom, 1971; Stull, 1988), the locally scaled gradients and turbulence statistics must become constants, independent of z or z/Λ. Nieuwstadt (1984) has shown that this is indeed the case for $z/\Lambda \gg 1$.

The practical utility of the local similarity theory predictions is somewhat questionable, because in order to predict velocity variances and the TKE one needs to know the local fluxes of momentum and heat, which are even more difficult to measure or estimate. Nevertheless, it provides a convenient framework of representing and comparing mean gradients and turbulence data in the SBL.

13.3 Mathematical Models of the PBL

Most of the quantitative PBL models are based on the fundamental laws of conservation of mass, energy, and momentum, which are expressed in the form of partial differential equations containing velocity, pressure, temperature or density, and concentrations of water vapor and trace gases, if needed. With the usual simplifying assumptions or approximations, these conservation equations have already been reviewed in Chapter 9. The difficulties in obtaining their particular or general solution using analytical and numerical methods have also been pointed out. Here, we further elaborate on some of the simpler first-order

closure, integral, and TKE closure models of the PBL, which are frequently used in practical applications of micrometeorology, as well as more sophisticated models employed in fundamental research on the PBL turbulence.

13.3.1 First-order closure models

For the idealized horizontally homogeneous PBL, in the absence of any active condensation and precipitation processes, the equations of mean motion and scalars reduce to the following:

$$\begin{aligned} \frac{\partial U}{\partial t} - f(V - V_g) &= -\frac{\partial \overline{uw}}{\partial z} \\ \frac{\partial V}{\partial t} + f(U - U_g) &= -\frac{\partial \overline{vw}}{\partial z} \end{aligned} \tag{13.16}$$

$$\begin{aligned} \frac{\partial \Theta}{\partial t} &= -\frac{\partial \overline{\theta w}}{\partial z} \\ \frac{\partial Q}{\partial t} &= -\frac{\partial \overline{qw}}{\partial z} \end{aligned} \tag{13.17}$$

in which horizontal pressure gradients have been expressed in terms of the specified geostrophic wind components U_g and V_g. The above equations for the horizontally homogeneous PBL still contain twice as many unknowns as the number of equations. Equations (13.16) of motion can further be simplified for the stationary flow by dropping the time-dependent terms; these terms are usually retained in scalar equations (13.17).

Local closure models In order to close the above set of equations of mean motion and other scalars, turbulent covariances or fluxes are expressed in terms of the gradients of mean velocity and scalars, using the eddy diffusivity and/or mixing length hypotheses introduced in Chapter 9. This type of closure is known as the local closure, because local fluxes are assumed to be related to only local gradients. The implied assumption and local closure models based on local gradient-transport hypotheses may be justified in the presence of large gradients as in the SBL, but not so in the presence of vanishingly small gradients that are usually encountered in the CBL. The basic premise of down-gradient transport becomes highly questionable and even invalid when large-scale convective motions dominate turbulent transports. It is a well-known fact that, in the convective mixed layer, the vertical momentum, heat, and water vapor fluxes are not related to the vanishingly small gradients of mean velocity, potential

temperature and specific humidity in that layer. In the neutral and stably stratified boundary layers with strong gradients of mean variables, however, there are no such conceptual difficulties, but eddy diffusivities and mixing lengths are specified largely on an ad hoc basis.

One can specify mixing length more rationally by identifying it with the characteristic large-eddy length scale which can be determined from measurements of turbulence. Both the mixing length and the large-eddy length scale are found to be proportional to the height above the surface, especially closer to the surface, and approach some constant values which are either proportional to the PBL depth or limited by stability in the upper part of the PBL. Simple interpolation formulas of the form

$$\frac{1}{l_m} = \frac{1}{kz} + \frac{1}{l_b} + \frac{1}{l_o} \tag{13.18}$$

have been proposed, in which $k \cong 0.4$ is the von Karman constant, l_b is a buoyancy-limited mixing length, and l_o is another limiting value which is assumed proportional to h, $u_*/|f|$, or $G_0/|f|$. The buoyancy-limited mixing length term is included only for modeling the SBL, in which l_b is taken proportional to either the Obukhov length L, or σ_w/N, where N is the Brunt–Vaisala frequency.

A comprehensive review of the many first-order local closure models that have been reported in the literature is given by Holt and Raman (1988). Some are based on explicit or implicit specification of eddy diffusivity profiles in the PBL. In most of the models eddy diffusivities are expressed in terms of a mixing length or large-eddy length scale whose profile (variation with height) in the PBL is then specified, as in Equation (13.18) or through other expression. The most commonly used relation between eddy viscosity and mixing length is of the form

$$K_m = l_m^2 \left| \frac{\partial \mathbf{V}}{\partial z} \right| f(\mathrm{Ri}) \tag{13.19}$$

where $f(\mathrm{Ri})$ is a decreasing function of Richardson number in the SBL, such that $f(0) = 1$.

As an example of a first-order closure model of the SBL, used in conjunction with the Rossby-number similarity scaling, Businger and Arya (1974) proposed the following expression for the normalized eddy viscosity $K_* = K_m f/u_*^2$:

$$K_* = k\xi(1 + \beta\xi\mu_*)^{-1} \exp(-|V_g/u_*|\xi) \tag{13.20}$$

where $\xi = fz/u_*$, $\mu_* = u_*/fL$, and $\beta \cong 5$ is an empirical constant. For the stationary (steady state) SBL, they expressed Equation (13.16) in the normalized form as

$$K_* \frac{d^2 T_x}{d\xi^2} + T_y = 0$$
$$K_* \frac{d^2 T_y}{d\xi^2} - T_x = 0 \tag{13.21}$$

in which $T_x = -\overline{uw}/u_*^2$ and $T_y = -\overline{vw}/u_*^2$ represent the normalized stresses in x and y directions, respectively.

The numerical solution of Equations (13.21) with K_* specified by Equation (13.20) yielded the vertical profiles of K_*, $(U - U_g)/u_*$, $(V - V_g)/u_*$, $\overline{uw}/u_*^2$, and $\overline{vw}/u_*^2$ for the various specified values of μ_* (Businger and Arya, 1974). The model results for the normalized eddy viscosity, shown in Figure 13.5, give some idea about the wide range of K_m values that may occur in the SBL, as well as about the strong dependence of K_m on height and stability. The model results of the PBL height (see Figure 13.6) also confirm the validity of Equations (13.7) and (13.8), although the implied value of $d \cong 0.7$ falls on the higher side of the empirical estimates. However, it also depends on the definition of the PBL height. Figure 13.6 shows that different heights represent different salient features of mean velocity and momentum flux profiles. The most satisfactory and frequently used definition is the height where the magnitude of the normalized stress reduces to an arbitrarily specified small fraction, e.g., 0.01 used by Businger and Arya (1974). The model estimated value of d will be smaller if a higher fraction (say, 0.05) is used for the normalized stress in defining the PBL height.

Figure 13.7 shows that ξ_τ, representing the normalized PBL height where shear stress falls to 1% of the surface stress, is uniquely related to the maximum dimensionless eddy viscosity ($K_{*\max}$). The best fitted line, also shown in the same figure, represents a simple power-law relationship, $\xi_\tau \cong 5.0 K_{*\max}^{0.55}$, which is not much different from that obtained from an analytical solution for a constant K_* (see Example Problem 1). The normalized stress profiles are found to be strongly dependent on the stability parameter μ_*, if they are represented as functions of fz/u_* (Businger and Arya, 1974). However, Figure 13.8 shows that the normalized stress profiles become essentially independent of μ_*, if they are represented as functions of z/h instead of ξ. This points to the merits of using the generalized similarity scaling, even for the SBL.

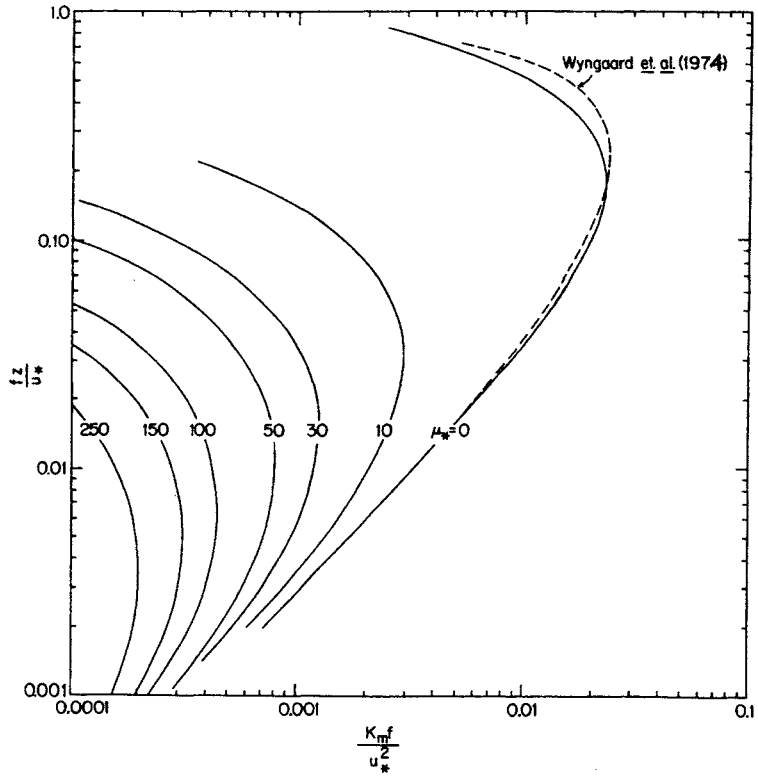

Figure 13.5 Model-predicted normalized eddy viscosity as a function of normalized height for different values of the stability parameter μ_*. The dashed curve is the result of the second-order closure model of Wyngaard *et al.* (1974) for the neutral PBL. [From Businger and Arya (1974).]

Example Problem 1

(a) Using the equations of mean motion in a stationary, horizontally homogeneous, and barotropic SBL, derive the corresponding equations (13.21) for the normalized stresses T_x and T_y.

(b) Obtain an analytical solution of Equations (13.21) for constant eddy diffusivity (K_*) and appropriate boundary conditions.

(c) Utilizing the above solution, calculate and compare the normalized stress profiles for $K_* = 0.002$ and 0.0002 representing slightly stable and moderately stable conditions, respectively. Also compare the dimensionless height of the SBL for the above two cases.

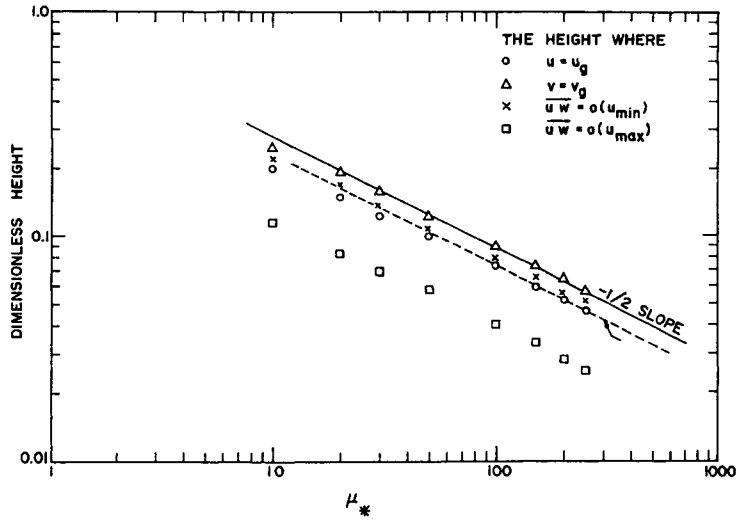

Figure 13.6 Dimensionless heights, representing salient features of mean velocity and momentum flux profiles in the SBL, as functions of stability parameter. The dashed line (indicated by arrow) represents Equation (13.8) with $d = 0.72$. [From Businger and Arya (1974).]

Solution

(a) For the stationary, horizontally homogeneous PBL, Equations (13.16) reduce to

$$-f(V - V_g) = -\frac{\partial \overline{uw}}{\partial z}$$

$$f(U - U_g) = -\frac{\partial \overline{vw}}{\partial z}$$

Differentiating these with respect to z and recognizing that in a barotropic PBL $\partial U_g/\partial z = 0$ and $\partial V_g/\partial z = 0$, we can write

$$-f\frac{\partial V}{\partial z} = -\frac{\partial^2 \overline{uw}}{\partial z^2}$$

$$f\frac{\partial U}{\partial z} = -\frac{\partial^2 \overline{vw}}{\partial z^2}$$

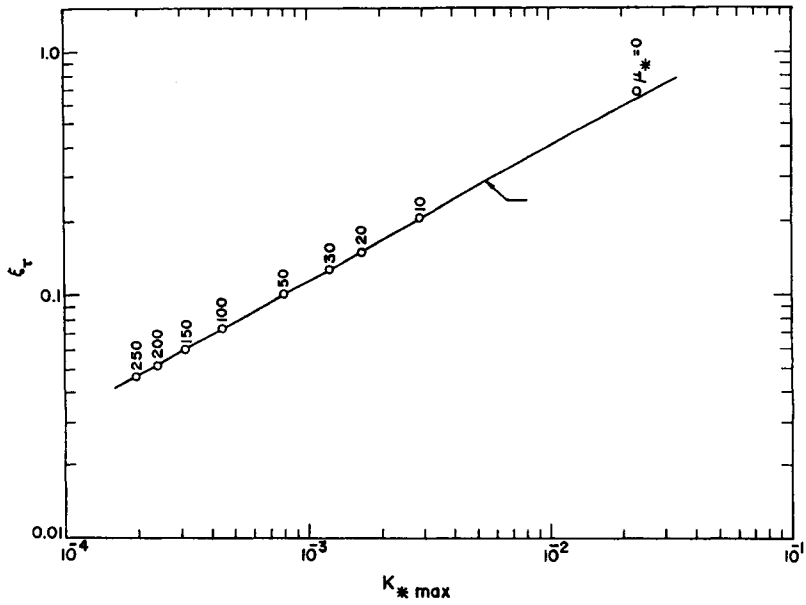

Figure 13.7 The dimensionless SBL height, where stress reduces to 1% of the surface stress, as a function of the maximum dimensionless eddy viscosity. The best-fitted line (indicated by arrow) represents a power-law relationship between the two parameters. [From Businger and Arya (1974).]

Multiplying both sides of equations by K_m and utilizing the eddy-viscosity hypothesis, the above equations can be expressed in terms of the momentum fluxes only as

$$f\overline{vw} = -\frac{\partial^2 \overline{uw}}{\partial z^2} K_m$$

$$-f\overline{uw} = -\frac{\partial^2 \overline{vw}}{\partial z^2} K_m$$

Now, using the normalized stresses $T_x = -\overline{uw}/u_*^2$ and $T_y = -\overline{vw}/u_*^2$ and the normalized height coordinate $\xi = fz/u_*$, the above equations are easily expressed in the form of Equations (13.21). Note that, in the above equations for the stationary and homogeneous PBL, partial derivatives can be written as ordinary derivatives.

(b) The solution of Equations (13.21) can more easily be obtained by combining the two coupled ordinary differential equations into one for the complex stress variable

$$T_c = T_x + iT_y$$

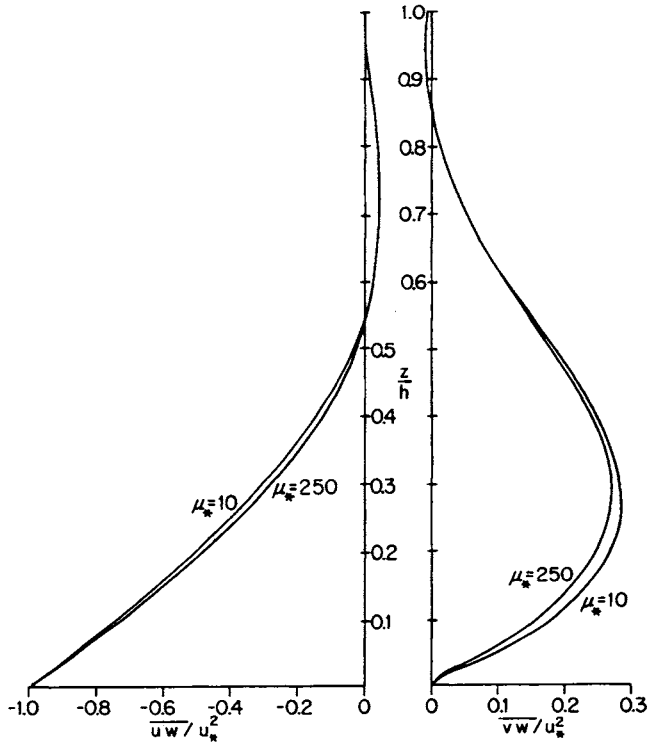

Figure 13.8 Normalized stresses (T_x and T_y) as functions of the normalized height (z/h) for $\mu_* = 10$ and 250, based on the numerical model results of Businger and Arya (1974).

We can follow the procedure used in Section 7.5 to express Equations (13.21) as

$$\frac{d^2T_c}{d\xi^2} - \frac{i}{K_*}T_c = 0$$

The particular solution satisfying the upper boundary condition that $T_c \to 0$ as $\xi \to \infty$, is given by

$$T_c = A\exp[-(1+i)a\xi]$$

where $a = (2K_*)^{-1/2}$, and A is a complex constant to be evaluated from the lower boundary condition. Here, we use a surface-layer coordinate system,

so that $T_c = 1$ at $\xi = 0$, which yields $A = 1$. Then, the above solution can be expressed as

$$T_x + iT_y = \exp(-a\xi)[\cos(a\xi) - i\sin(a\xi)]$$

so that,

$$T_x = \exp(-a\xi)\cos(a\xi)$$
$$T_y = -\exp(-a\xi)\sin(a\xi)$$

and the total stress

$$T = (T_x^2 + T_y^2)^{1/2} = \exp(-a\xi)$$

(c) According to the above solution, the total stress decreases exponentially with the normalized height $a\xi$, while the two components (T_x and T_y) are modulated by $\cos(a\xi)$ and $-\sin(a\xi)$ terms, respectively. The stress profiles are self-similar in terms of the modified similarity parameter $a\xi$ which is proportional to the ratio ξ/ξ_τ, where $\xi_\tau = fh/u_*$ is the dimensionless PBL height where the stress has decreased to about 1% of the surface value (i.e., $T = 0.01$). From the exponential decrease of stress, it is easy to see that

$$\xi_\tau \cong 4.6\sqrt{2K_*} \cong 6.51K_*^{1/2}$$

which gives the values of $\xi_\tau \cong 0.29$ and 0.09 for the slightly stable ($K_* = 0.002$) and moderately stable ($K_* = 0.0002$) cases, respectively. Note that the heights where the stress has decreased to only 5% of the surface stress are 35% smaller than the above values of ξ_τ.

Nonlocal closure models Recognizing the limitations of local closure hypotheses, especially under unstable and convective conditions, several nonlocal closure formulations have been proposed for modeling mixing processes in the CBL (Stull, 1988, 1993; Pleim and Chang, 1992). Nonlocal closures are based on the basic premise that turbulent eddies of varying sizes can transport flow properties, such as momentum, heat and mass, across finite vertical distances, comparable to their size. Thus, the largest eddies in the CBL with the vertical dimension equal to the PBL depth h, can transfer properties all the way from the surface layer to the top of the CBL and vice versa, irrespective of the vanishingly small gradients in the mixed layer. Consequently, mean velocity, potential temperature, and scalar concentrations at any location (height level) are a result of eddy transport and mixing of fluid parcels coming from many cross-stream locations (height levels).

Stull (1993) has proposed a transilient turbulence model of nonlocal mixing across finite distances. In this, a vertical column of air is assumed to be divided between a finite number (N) of equal size grid boxes. Turbulent mixing of fluid coming from any box (denoted by index j) into the reference grid box (denoted by index i) can change any conserved passive scalar property $\tilde{s}_i$ (e.g., potential temperature, specific humidity, etc.) of the reference box. If c_{ij} represents the fraction of air in box i that came from box j during a time interval Δt, one can express the mean value of $\tilde{s}_i$ at a future time as

$$S_i(t + \Delta t) = \sum_{j=1}^{N} c_{ij}(t, \Delta t) S_j(t) \tag{13.22}$$

in which the matrix of mixing coefficients c_{ij} is called the transilient matrix. By definition, the conservation of the transferred property requires that

$$\sum_{j=1}^{N} c_{ij} = \sum_{i=1}^{N} c_{ij} = 1 \tag{13.23}$$

The vertical turbulent flux of scalar at any height k (defined as the top of the grid box k) is given by

$$\overline{ws}(k) = \frac{\Delta z}{\Delta t} \sum_{i=1}^{k} \sum_{j=1}^{N} c_{ij}(S_i - S_j) \tag{13.24}$$

where Δz is the vertical grid spacing and Δt is time step for the $c_{ij}(t, \Delta t)$ matrix. The above discrete-grid expression can also be written in a continuous form (Stull, 1988).

The main closure problem in the above model is the specification or estimation of the transilient matrix c_{ij}. These mixing coefficients are expected to be different for different flow situations and cannot be generalized. Different approaches have been suggested for estimating the mixing coefficients, but none of them is very rigorous and completely satisfactory (Stull, 1988, 1993). For example, one approach utilizes the nonlocal (integral) form of the turbulent kinetic energy equation. After parameterizing the unknown terms in terms of the mean wind and potential temperature parameters, mixing potentials are obtained and c_{ij} are, then, expressed in terms of mixing potentials. The more non-zero elements of matrix in the model, the more complex and expensive would be the numerical solution.

Another approach aimed at reducing the computational cost is to specify the transilient matrix according to some simple conceptual model of mixing in the

CBL (Pleim and Chang, 1992). In this way, only a fraction of the elements in the transilient matrix need to be nonzero. Both symmetric and asymmetric convective mixing models have been proposed. For example, in the asymmetric convective mixing (ACM) model proposed by Pleim and Chang (1992) the upward transport originates in the bottom-most layer, which constitutes the surface layer, from which air is allowed to mix with each of the upper layers in the CBL directly. The downward transport and mixing, on the other hand, proceed from each layer to the next lower layer only in a cascading manner. This simulates rapid upward transport from the surface layer by buoyant plumes and more gradual compensatory subsidence in downdrafts. The ACM model has been shown to perform much better than some of the local closure schemes including the one based on the turbulence kinetic energy equation (Alapaty *et al.*, 1997).

Integral models Integral or slab models use the vertically integrated or layer-averaged forms of equations of motion and thermodynamic variables (Driedonks, 1982; Arya and Byun, 1987; Stull, 1988):

$$\begin{aligned}\frac{\partial U_{\mathrm{m}}}{\partial t} &= f(V_{\mathrm{m}} - V_{\mathrm{gm}}) + \frac{1}{h}[(\overline{uw})_0 - (\overline{uw})_h] \\ \frac{\partial V_{\mathrm{m}}}{\partial t} &= -f(U_{\mathrm{m}} - U_{\mathrm{gm}}) + \frac{1}{h}[(\overline{vw})_0 - (\overline{vw})_h]\end{aligned} \tag{13.25}$$

$$\frac{\partial \Theta_{\mathrm{m}}}{\partial t} = \frac{1}{h}[(\overline{w\theta})_0 - (\overline{w\theta})_h] \tag{13.26}$$

in which the subscript m denotes the layer-averaged value for the mixed layer, e.g.,

$$\Theta_{\mathrm{m}} = \frac{1}{h}\int_0^h \Theta \, dz \tag{13.27}$$

The above equations for the layer-averaged wind components (U_{m}, V_{m}) and potential temperature (Θ_{m}), also contain the surface fluxes of momentum and heat, and those at the top of the mixed layer or the PBL. The surface fluxes can be parameterized through the usual bulk transfer relations. The fluxes at the top

of the mixed layer are parameterized through the following entrainment relations:

$$\begin{aligned} (\overline{uw})_h &= -w_e \Delta U \\ (\overline{vw})_h &= -w_e \Delta V \\ (\overline{\theta w})_h &= -w_e \Delta \Theta \end{aligned} \tag{13.28}$$

in which ΔU, ΔV, and $\Delta\Theta$ denote the jumps in U, V, and Θ across the interface or the transition layer, and w_e is the entrainment velocity which is intimately related to the rate of growth of the mixed layer as

$$\frac{\partial h}{\partial t} = w_e + W_h \tag{13.29}$$

Note that $w_e = \partial h/\partial t$ in the absence of any mean vertical velocity (W_h) at the top of the mixed layer; it represents the volume of air entrained into the top of the mixed layer per unit horizontal area per unit time.

The entrainment relations (13.28)–(13.29), in conjunction with the usual parameterization of the surface fluxes provide the necessary closure to the set of equations which can be numerically solved. In addition, the rate equations for the mixed layer depth or the PBL height, transition-layer thickness, and changes or jumps in the mean variables across the transition layer are also carried in some integral models. Depending on the sophistication with which the transition or entrainment layer at the top of the mixed layer is represented, the various zeroth-order and first-order slab models have been proposed for the horizontally homogeneous CBL (Driedonks, 1982; Arya and Byun, 1987; Stull, 1988). Simpler zeroth-order jump models may be adequate for predicting the mixed-layer depth and potential temperature, but more sophisticated integral models are required for better simulation of the thickness of and entrainment processes occurring in the transition layer.

The most widely used application of integral modeling has been in the development of mixed-layer height models of varying degrees of sophistication. The evolution of the mixed-layer depth over heated land surfaces during the day occurs in several stages or phases (Stull, 1988, Chapter 11): (1) the erosion or burning off of the nocturnal inversion and formation of a shallow mixed layer which slowly deepens in early morning hours after sunrise; (2) rapid growth of the mixed layer during the mid-morning period; (3) slow growth of the deep mixed layer in the afternoon period; and (4) decay of turbulence in the mixed layer of nearly constant depth during the late afternoon and evening transition period.

No simple integral model can faithfully simulate all the above stages of mixed-layer depth evolution. However, even some crude models have been shown to simulate, approximately, the mixed-layer growth during most of the daytime period, especially under fair-weather, clear sky conditions. For example, the thermodynamic method or model of mixed-layer growth is based on thermodynamic considerations only, while the dynamics of turbulent entrainment is neglected. The rate of growth of mixed-layer depth is simply related (proportional) to the rate of warming of the mixed layer as

$$\frac{\partial h}{\partial t} = \frac{1}{\gamma}\frac{\partial \Theta_m}{\partial t} \tag{13.30}$$

where $\gamma = \partial\Theta/\partial z$ is the potential temperature gradient above the top of the mixed layer.

Substituting from Equation (13.26) into Equation (13.30), one obtains

$$\frac{\partial h}{\partial t} = \frac{1}{\gamma h}[(\overline{w\theta})_0 - (\overline{w\theta})_h]$$

or (13.31)

$$\frac{\partial h^2}{\partial t} = \frac{2}{\gamma}[(\overline{w\theta})_0 - (\overline{w\theta})_h]$$

Parameterizing the entrainment heat flux simply as a fraction of the surface heat flux, i.e.,

$$(\overline{w\theta})_h = -C(\overline{w\theta})_0 \tag{13.32}$$

and integrating Equation (13.31), one can obtain the following expression for the evolution of the mixed-layer depth:

$$h(t) = \left[h_0^2 + 2\int_{t_0}^{t} \frac{(1+C)}{\gamma}(\overline{w\theta})_0\, dt\right]^{1/2} \tag{13.33}$$

in which h_0 is the initial depth at time t_0. The integral can be evaluated numerically if C, γ, and $(\overline{w\theta})_0$ can be specified as functions of time. In the simplest case, C and γ are assumed constants (e.g., $C \cong 0.2$ and γ can be estimated from the initial temperature sounding at $t = t_0$ which can also be used to estimate h_0), so that Equation (13.33) can be simplified as

$$h(t) = \left[h_0^2 + \frac{2(1+C)}{\gamma}\int_{t_0}^{t} (\overline{w\theta})_0\, dt\right]^{1/2} \tag{13.34}$$

Thus, according to this thermodynamic model, the mixed-layer depth at any time essentially depends on the strength of the inversion above and the accumulation of surface heat flux up to that time. The most important parameter in this model is $(\overline{w\theta})_0/\gamma$ and its variation with time; it may vary from 0 to 10^5 m^2 h^{-1} with the maximum occurring near midday.

The integral of the surface heat flux in Equation (13.34) can easily be evaluated for the specified $(\overline{w\theta})_0$ as a function of time. For the special case of constant heat flux, which may be typical of overcast conditions, Equation (13.34) yields

$$h(t) = \left[h_0^2 + \frac{2}{\gamma}(1 + C)(\overline{w\theta})_0(t - t_0)\right]^{1/2} \tag{13.35}$$

For the more common fair-weather conditions, the surface heat flux may be expressed as a half-cosine wave function whose integral is also readily obtained.

Even though the simple thermodynamic model described above neglects the dynamics of turbulent entrainment, it is found to explain roughly 80–90% of the observed variation of the mixed-layer depth. Other more sophisticated mixed-layer height or depth models have also been proposed in the literature (Driedonks, 1982; Arya and Byun, 1987; Stull, 1988, Chapter 11). They mostly differ in the representation of the entrainment or transition layer and the parameterization of entrainment velocity.

Example Problem 2

Using the thermodynamic model of mixed-layer growth during the daytime unstable and convective conditions, calculate and compare the evolutions of the mixed-layer height with time after the breakup of the surface inversion at 10 AM, when the mixed layer was 200 m deep, for the following conditions:

(a) overcast skies with a constant surface heat flux of 150 W m^{-2} throughout the 12 h daylight period and $\gamma = 0.02$ K m^{-1};

(b) clear skies with a sinusoidally varying heat flux with its maximum value of 300 W m^{-2} at 2 PM (14 h), and a capping inversion with a constant potential temperature gradient of 0.02 K m^{-1}.

Solution

(a) For this case we can use Equation (13.35) in which $h_0 = 200$ m, $(\overline{w\theta})_0 = 150/1200 = 0.125$ K m s^{-1}, $\gamma = 0.02$ K m^{-1}, $(\overline{w\theta})_0/\gamma = 22\,500$ m^2 h^{-1}, and $t_0 = 10$ h. Assuming $C = 0.2$, the mixed-layer height is given by

$$h(t) = [40\,000 + 54\,000(t - t_0)]^{1/2}$$

which is used to calculate the following results:

t (h):	10	12	14	16	18	20
h (m):	200	385	506	603	687	762

(b) The surface heat flux can be expressed as

$$(\overline{w\theta})_0 = (\overline{w\theta})_{\max} \sin[\pi(t-8)/12]$$

in which $(\overline{w\theta})_{\max} = 300/1200 = 0.25$ K m s^{-1}.

Substituting the above expression in Equation (13.34), we get

$$h(t) = [40\,000 + 108\,000 \int_{10}^{t} \sin[\pi(t-8)/12]dt]^{1/2}$$
$$= [40\,000 + 108\,000 I(t)]^{1/2}$$

in which the integral function $I(t)$ can be evaluated as

$$I(t) = \frac{12}{\pi}\left[\cos\frac{\pi}{6} - \cos\frac{\pi(t-8)}{12}\right]$$

The results of calculations are as follows:

t (h):	10	12	14	16	18	20
$I(t)$:	0	1.398	3.308	5.186	6.616	7.128
$h(t)$:	200	437	630	775	869	900

Comparing the model-predicted results for the two cases, it is clear that more rapid development of the mixed layer occurs during the clear sky conditions with sinusoidally varying surface heat flux.

13.3.2 Turbulent kinetic energy models

In the first-order local closure models, one has to specify eddy diffusivities or mixing lengths as functions of the characteristic length and velocity scales of turbulence. The most appropriate dynamical equation for the turbulence

velocity scale, which can be taken as the square-root of TKE, is Equation (9.10) which can further be simplified for the horizontally homogeneous PBL as

$$\frac{\partial E}{\partial t} = -\left[\overline{uw}\frac{\partial U}{\partial z} + \overline{vw}\frac{\partial V}{\partial z}\right] + \frac{g}{T_{vo}}\overline{w\theta_v} - \frac{\partial}{\partial z}\left(\overline{we} + \frac{\overline{wp}}{\rho_o}\right) - \varepsilon \tag{13.36}$$

All the TKE models contain Equation (13.36), in addition to the equations for mean variables, in which turbulent fluxes or covariances are parameterized using the usual first-order closure relations. Thus, the turbulent transport term is parameterized as

$$\overline{we} + \frac{\overline{wp}}{\rho_o} = -K_E\frac{\partial E}{\partial z} \tag{13.37}$$

where K_E is the TKE diffusivity which is assumed equal or proportional to K_m. In the parameterized form Equation (13.36) can be written as

$$\frac{\partial E}{\partial t} = K_m\left[\left(\frac{\partial U}{\partial z}\right) + \left(\frac{\partial V}{\partial z}\right)^2\right] - \frac{g}{T_{vo}}K_h\frac{\partial \theta_v}{\partial z} + \frac{\partial}{\partial z}\left(K_E\frac{\partial E}{\partial z}\right) - \varepsilon \tag{13.38}$$

in which the ratios of eddy diffusivities, viz., $\sigma_h = K_m/K_h$ and $\sigma_E = K_m/K_E$, are generally specified as constants (e.g., $\sigma_h = 0.9$ and $\sigma_E = 1$ are the widely used standard values). The closure is still not complete without the specification of K_m and ε. Different approaches or models have been used for this purpose.

The parameterized length-scale model The simplest parameterizations of eddy viscosity and the rate of energy dissipation are based on the TKE and appropriate length scales; the most commonly used parametric relations are:

$$K_m = C\ell E^{1/2} \tag{13.39}$$

$$\varepsilon = C_\varepsilon E^{3/2}/\ell_\varepsilon \tag{13.40}$$

Here, ℓ is the large-eddy length scale, ℓ_ε is the dissipation length scale, and C and C_ε are empirical constants whose values may depend on how ℓ and ℓ_ε are specified. In most of the TKE models it is assumed that $\ell_\varepsilon = \ell = l_m$, where the mixing length is usually specified as in Equation (13.18), while a few investigators have used different expressions for ℓ and ℓ_ε (Therry and Lacarrere, 1983).

Substituting from the well-known similarity relations for the various parameters in the neutral surface layer (e.g., $K_m = kzu_*$, $\varepsilon = u_*^3/kz$, $\ell = \ell_\varepsilon = kz$, and $E \cong 5.5u_*^2$), one can estimate $C \cong 0.43$ and $C_\varepsilon = C^3 \cong 0.08$. Somewhat different

values of these constants might be more appropriate when modeling the entire PBL under different stability conditions (Detering and Etling, 1985; Lacser and Arya, 1986).

A wide variety of length-scale parameterizations have been proposed in the literature (Holt and Raman, 1988). Sensitivity tests, including a comparative study of several different parameterizations, have shown that, while mean wind and temperature profiles may not be very sensitive to different formulations, the TKE and the rate of energy dissipation are quite sensitive to the same (Lacser and Arya, 1986).

The E–ε *model* In most computational fluid dynamics (CFD) models of turbulent flows, the dynamical equation for the rate of energy dissipation is carried in addition to the TKE equation. In these so-called k–ε or E–ε models, the eddy viscosity is usually expressed (parameterized) in terms of E and ε as

$$K_m = C_k E^2/\varepsilon \tag{13.41}$$

Where C_k is an empirical constant that may actually depend on the type of flow, e.g., for the neutral surface layer, $C_k \cong 0.033$. The derivation of the dynamical equation for ε is quite involved (Lumley, 1980); it contains many new unknown terms that are considerably simplified and parameterized. The highly parameterized form used in the standard E–ε model is given as

$$\frac{\partial \varepsilon}{\partial t} = C_1 \frac{\varepsilon}{E}\left[-\overline{uw}\frac{\partial U}{\partial z} - \overline{vw}\frac{\partial V}{\partial z} + \frac{g}{T_{vo}}\overline{\theta_v w}\right] - C_2\frac{\varepsilon^2}{E} + \frac{\partial}{\partial z}\left(K_\varepsilon \frac{\partial \varepsilon}{\partial z}\right) \tag{13.42}$$

where C_1 and C_2 are empirical constants, and K_ε is the diffusivity of dissipation rate which is usually linked to that of momentum as $K_\varepsilon = K_m/\sigma_\varepsilon$, where σ_ε is another diffusivity ratio.

The various terms on the right-hand side of Equation (13.42) represent production, destruction and turbulent transport of the dissipation rate respectively. In their parameterized forms, represented in Equation (13.42), the production and destruction terms have been simply assumed to be proportional to the production and dissipation of the TKE. The various constants (C_k, C_1, C_2, etc.) in the E–ε model, often used in commercial CFD codes, have been estimated from the laboratory experimental data. Their 'standard' values ($C_k = 0.09$, $C_1 = 1.44$, $C_2 = 1.92$, etc.) may not be appropriate for the stratified, rotating atmospheric PBL (Detering and Etling, 1985). But sufficiently accurate measurements of the various terms in E and ε equations are not available for a direct empirical determination of these constants for the PBL. Different values have been suggested by different investigators on the basis of

comparisons of model-predicted and observed winds and turbulence (Holt and Raman, 1988).

The ε–ℓ model In this model the eddy viscosity is determined by Equation (13.39), with both E and ℓ computed from their dynamical equations. Thus, instead of the ε equation, a prognostic equation for the length scale ℓ (more appropriately, the product $E\ell$) is included in the model. Mellor and Yamada (1974) proposed such a model as a compromise between their level 2 and level 3 models. The parameterized form of the prognostic equation for $E\ell$ looks similar to that for the dissipation rate ε (Mellor and Yamada, 1982); both have the same limitations and large uncertainties in the estimates of the various closure constants.

A comparison of different TKE closure schemes with limited field experimental data by Holt and Raman (1988) reveals that mean profiles of wind, potential temperature, and specific humidity show little sensitivity to the type of closure scheme. Thus, in the determination of K_m, using a diagnostic formulation of ℓ or a prognostic determination of ε makes very little difference. However, the E–ε model performs best in the simulation of turbulence structure, because the energy dissipation rate is calculated from its prognostic equation rather than simply parameterized by Equation (13.40) with a specified length scale.

13.3.3 Higher-order closure models

The gradient transport theory with local closure relations has some serious flaws and becomes invalid in convective conditions when turbulent transports are not necessarily down the mean gradients. Most of the TKE closure models also utilize the local gradient-transport concept and relations and, hence, fail to account for significant counter-gradient transports by large convective eddies. For this reason, second- and higher-order closure models of turbulence and diffusion in the PBL have also been proposed (Mellor and Yamada, 1974; Wyngaard *et al.*, 1974; Andre *et al.*, 1978; Lumley, 1980). Second-order closure models are based on the dynamical equations for turbulent transports or fluxes (Stull, 1988; Sorbjan, 1989). These equations contain the unknown third moments, correlations involving pressure and velocity or other scalar fluctuations, and the molecular dissipation terms, all of which have to be parameterized to close the set of equations. Thus, the closure problem shifts to the higher-order second-moment equations.

The second-moment equations contain much more physics of turbulent transports than the TKE equation. Therefore, it has been argued that the second-order closure approach should be more general and accurate than the

first-order or one-and-a-half-order (TKE) closure approach. Similarly, a third-order closure model utilizing the dynamical equations for all the first, second and third moments might be considered even more general, because it contains more physics of turbulence. Unfortunately, the governing equations also become more complex and numerous, and their closure becomes much more difficult and ad hoc in the absence of experimental data on higher moments of turbulence (Andre *et al.*, 1978). Here we mention only some of the commonly used closure approaches to parameterize the turbulent transport (third moments), molecular dissipation, and pressure terms in the second-moment equations.

The third-moment terms, representing turbulent transports of second moments, are very important to the dynamics of buoyancy-driven unstable and convective boundary layers. They are found to be rather insignificant in stably stratified flows, such as the SBL. The simplest parameterization of turbulent transport terms is based on the gradient-transport concept, whereby third moments are expressed as products of the spatial gradients of second moments and some form of turbulent diffusivity. The diffusivity is expressed in terms of large-eddy length and velocity scales (e.g., $K \sim E^{1/2}\ell$). Alternatively, the turbulent diffusion time scale defined by the ratio E/ε can be used (e.g., $K \sim E^2/\varepsilon$). However, this type of turbulent-transport modeling has been found to be deficient and inconsistent with the observed turbulence structure in the CBL. A more complex, but general, functional-expansion approach (Lumley, 1980) can remove some of the limitations of the simpler approach, but it also introduces many more terms and empirical constants in the parametric relations.

An accurate representation or parameterization of molecular dissipation terms in second-moment equations, especially the variance equations, is important, because these terms determine the rate at which turbulence variances and the TKE are destroyed. In some models, ε also determines the turbulence length and time scales that are used in the parameterization of turbulent transport and pressure terms. In the simplest approach, dissipations are expressed in terms of the appropriate length and velocity scales as in Equation (13.40). Alternatively, dynamical equations are carried for the rates of dissipation of TKE and variances of scalar fluctuations. Such equations are very complex and only the highly simplified and parameterized forms are used in second-order closure models (Wyngaard *et al.*, 1974; Lumley, 1980). The molecular dissipation terms in the dynamical equations for the covariances or turbulent fluxes are usually neglected, using Kolmogorov's local isotropy hypothesis for large-Reynolds-number flows.

The satisfactory parameterization of the covariances between pressure fluctuations and spatial gradients of velocity, temperature, and other scalar fluctuations, which are also called return-to-isotropy terms, is probably the

most difficult and challenging problem in higher-order closure modeling. These are the primary destruction terms in the covariance equations; they are also responsible for the distribution of turbulence kinetic energy among three components. In the simplest parameterizations, pressure terms are assumed to be proportional to the second moments (variances and covariances) they tend to destroy. But this approach does not properly account for the interactions of turbulence with mean flow shear and buoyancy. More refined parameterizations can account for the above interactions approximately, but contain many more terms and empirical constants.

Higher-order closure models provide a great deal of additional information on turbulence variances and covariances that cannot be obtained from any first-order closure model. This information is particularly useful in applications of micrometeorology to turbulent exchange and transport processes in the PBL. Higher-order closure models also permit counter-gradient transports under convective conditions, although only after introducing additional terms representing buoyancy-induced motions and mixing.

The major limitations of the second- and higher-order closure approach are the increasingly large number of dynamical equations for the second and higher moments that have to be solved and the lack of general validity and uniqueness of closure relations that have been developed and used. Some of the closure relations have been validated and closure constants evaluated using laboratory experimental data from near-neutral, nonrotating, turbulent shear flows. The same relations and values of empirical constants may not be applicable to the atmospheric PBL in which buoyancy and rotational effects are particularly important. There are too many closure constants of which only a few can be estimated from the available experimental data. This limitation becomes more and more severe as the order of closure is increased. Only limited measurements of third and fourth moments of turbulence in the atmosphere are available and large uncertainties in them do not permit their use in validating closure relations and empirically evaluating the various constants.

A major limitation of all the ensemble-averaged turbulence closure models is that ensemble averaging forces one to parameterize the effects of the entire spectrum of eddy motions, including the large energy-containing eddies. These large eddies in a turbulent flow are very sensitive to the geometry of flow, as well as to the dominant mechanisms of production and destruction of turbulence in the flow. Therefore, some of the turbulence modelers have expressed doubt whether any higher-order closure model could be applied to the wide range of conditions encountered in the atmosphere. With increasing computer power and widespread use of computer networks, large-eddy simulation of turbulence is likely to become a more practical and economically feasible modeling approach.

13.3.4 Large-eddy simulations

The large-eddy simulation (LES) approach to turbulence modeling has been briefly introduced in Chapter 9. Here we describe some aspects of grid-volume averaging of the equations of motion, the subgrid-scale (SGS) parameterizations or models that are invariably used in LES, and some results of large-eddy simulations of neutral, unstable, and stable atmosphere boundary layers. Merits and limitations of the LES approach will also be discussed.

Grid-volume-averaged equations An appropriate set of equations of motion, potential temperature and other scalar variables to be used in LES can be obtained by grid-volume averaging of the instantaneous equations. This operation is similar to ensemble averaging and utilizes the same Reynolds averaging rules or conditions as discussed in Chapter 9. But there are also some subtle and conceptual differences as discussed by Mason (1994). Grid-volume averaging amounts to applying a spatial filter which, for all practical purposes, is determined by the grid resolution used in the model. The optimum filter is not necessarily the one with sharp cutoffs at grid boundaries; such a filter was used by Deardorff (1972a, 1973). Gaussian and other smooth spatial filters have been found to be more efficient for mathematical operations.

If we define the grid-volume averaging or the spatial filter operation so that the average variables are denoted by an overbar and the SGS fluctuations around averages are denoted by a prime, instantaneous variables in Equations (9.1) can be expressed as

$$\begin{aligned} \tilde{u} &= \bar{u} + u', \ \tilde{v} = \bar{v} + v' \\ \tilde{w} &= \bar{w} + w', \ \tilde{\theta} = \bar{\theta} + \theta' \end{aligned} \tag{13.43}$$

and so on. Then, substituting from Equations (13.43) into (9.1) and averaging over each grid volume yields the grid-volume-averaged equations. For spatial filters preserving the average values of variables upon second-filter operation (e.g., $\bar{\bar{u}} = \bar{u}$, etc.), the filtered equations have exactly the same forms as ensemble-averaged equations (9.8), except for the difference in our notation of ensemble-averaged and grid-volume-averaged (filtered) variables. Thus, the latter can be written as

$$\frac{\partial \bar{u}}{\partial x} + \frac{\partial \bar{v}}{\partial y} + \frac{\partial \bar{w}}{\partial z} = 0 \tag{13.44}$$

$$\frac{\partial \bar{u}}{\partial t} + \frac{\partial(\bar{u}\bar{u})}{\partial x} + \frac{\partial(\bar{u}\bar{v})}{\partial y} + \frac{\partial(\bar{u}\bar{w})}{\partial z} - f\bar{v} = -\frac{1}{\rho_o}\frac{\partial \bar{p}_1}{\partial x} + \nu\nabla^2\bar{u} + \left(\frac{\partial \tau_{xx}}{\partial x} + \frac{\partial \tau_{xy}}{\partial y} + \frac{\partial \tau_{xz}}{\partial z}\right) \tag{13.45}$$

and so on for $\bar{v}$, $\bar{w}$, and $\bar{\theta}$. The Reynolds stresses on the right-hand side can, in general, be expressed as

$$\tau_{ij} = -\left(\overline{\bar{u}_i\bar{u}_j} - \bar{u}_i\bar{u}_j\right) \tag{13.46}$$

in which the indices i and j can take on values of 1, 2 and 3 to represent the velocity components ($u_1 = u$, $u_2 = v$, and $u_3 = w$) in the three directions ($x_1 = x$, $x_2 = y$, $x_3 = z$), using the Cartesian frame of reference.

The Reynolds stresses in the above LES equations essentially represent the contributions of subgrid-scale motions. This can easily be seen from the Reynolds decomposition of instantaneous variables and by expressing the grid-volume-averaged momentum flux as

$$\begin{aligned}\overline{\bar{u}_i\bar{u}_j} &= \overline{(\bar{u}_i + u_i')(\bar{u}_j + u_j')} \\ &= \overline{\bar{u}_i\bar{u}_j} + \overline{\bar{u}_i u_j'} + \overline{u_i'\bar{u}_j} + \overline{u_i'u_j'}\end{aligned} \tag{13.47}$$

Note that the first term on the right-hand side of Equation (13.47) may not be much different from $\bar{u}_i\bar{u}_j$, so that τ_{ij} largely consists of SGS contributions. It should be recognized, however, that the resolved LES variables $\bar{u}$. $\bar{v}$, etc., also include the random turbulent fluctuations in both space and time that are due to large-eddy motions with scales larger than the filter or grid size. The SGS stresses or fluxes also have this random variability, but on average, their magnitudes are much smaller than the ensemble-averaged Reynolds fluxes, because the former contain only minor contributions of SGS motions.

For the more general filter operations that may not preserve previously filtered average variables on a second filter operation or averaging, i.e., for which $\bar{\bar{u}} \neq \bar{u}$, etc., additional terms are generated by the averaging or filter operation on the instantaneous equations. We will not consider such filters here, but simply state that the grid-volume-averaged or filtered equations of conservation of mass, momentum, etc., used in LES are still expressed in the same forms as Equations (13.44) and (13.45), but each of the SGS flux terms contain different types of SGS contributions as indicated by Equations (13.46) and (13.47).

Subgrid-scale models In order to close the set of grid-volume-averaged or filtered equations, the unknown SGS Reynolds stresses and fluxes must be

parameterized in terms of the resolved variables for which the set of LES equations is numerically solved. The various SGS closure models have been proposed in the literature; these have been reviewed by, among others, Deardorff (1973), Ferziger (1993), and Mason (1994). Here, we briefly describe only a few widely used, simple SGS models.

The simplest and the oldest SGS model is that proposed by Smagorinski (1963) in the context of general circulation modeling. The Smagorinski model is essentially a first-order closure model based on the classical Boussinesq concept of eddy viscosity, but applied to SGS fluxes. Using the generalized gradient-transport relationship with a scalar SGS eddy viscosity K, the Reynolds stresses can be expressed as

$$\tau_{ij} = K\left(\frac{\partial \bar{u}_i}{\partial x_j} + \frac{\partial \bar{u}_j}{\partial x_i}\right) = 2KS_{ij} \tag{13.48}$$

in which S_{ij} denotes the rate of SGS deformation.

The SGS eddy viscosity in Equation (13.48) should be distinguished from the overall eddy viscosity introduced in Chapter 9. Even when the ensemble-averaged fluxes may not be down gradient, as often occurs in the convective mixed layer, due to the presence of large-eddy convective motions, it is reasonable to expect that the gradient-transport hypothesis might be more generally valid for small-scale (SGS) motions. Indeed, Equation (13.48) can be derived in several different ways and not just heuristically as Smagorinski did in 1963 (Ferziger, 1993). These derivations suggest that the SGS eddy viscosity can be expressed as

$$K = \ell_o^2 S \tag{13.49}$$

$$S^2 = \frac{1}{2}\left(\frac{\partial \bar{u}_i}{\partial x_j} + \frac{\partial \bar{u}_j}{\partial x_i}\right)^2 \tag{13.50}$$

where ℓ_o is the SGS mixing-length scale which is related to filter scale ℓ_f, or the geometric mean grid size

$$\Delta = (\Delta x \Delta y \Delta z)^{1/3} \tag{13.51}$$

Deardorff (1972a) used the simplest proportionality relation for the mixing length

$$\ell_o = C_s \Delta \tag{13.52}$$

in which the value of Smagorinski constant C_s is found to be somewhat dependent on mean flow shear, stability, proximity to the surface, and possibly other factors. For example, the optimum values of $C_s = 0.13$ and 0.21 were found by Deardorff (1972a) for the neutral and unstable PBLs, respectively, using his sharp cutoff filter.

A different analysis by Mason (1994) with a spherical filter of scale ℓ_f yields the following expression for ℓ_o:

$$\ell_o = C_f \ell_f \tag{13.53}$$

where $C_f \cong 0.17$. The precise value of C_f, in general, must depend on the filter shape. It is clear from Equations (13.52) and (13.53) that when the filter scale is equal to the average grid size, $C_s = C_f$. Mason has shown that $\ell_f = \Delta$ with $C_s = C_f \cong 0.2$ is indeed the optimum choice of filter scale.

In large-eddy simulations of the atmospheric boundary layer one should also be concerned about the possible effects of buoyancy or stability on the SGS model. If the filter scale or the mean grid size actually falls within the locally isotropic range of eddy sizes, then one would expect a negligible influence of buoyancy on the SGS model. The SGS model should also include a parametric relation for the SGS heat flux similar to that of the Reynolds stress. The corresponding SGS diffusivity of heat K_h may differ from that of momentum. The commonly used assumption is $K_h = \alpha K_m$, in which $\alpha = 1$ to 3, depending on the PBL stability and the type of filter used in the LES (Deardorff, 1972a; Mason, 1994). This procedure appears to be well justified for simulating unstable and convective boundary layers (for these $\alpha > 1$), but may not be adequate in the stably stratified transition layer lying above the convective mixed layer.

In the LES of stably stratified flows including the SBL, the theoretical requirement of a small grid size, so that all SGS motions are locally isotropic, is unlikely to be achieved, and some direct effect of stability must be incorporated in the SGS model. For example, Deardorff (1973) used an equation of the subgrid turbulence kinetic energy and derived an expression for the SGS eddy viscosity that is dependent on the flux Richardson number. However, this amounts to a higher-order TKE closure in which the subgrid-scale TKE equation is included in the model, with the usual parameterizations of $\varepsilon \sim E^{3/2}/\ell$, $K_m \sim E^{1/2}\ell$, etc. The simpler approach of using a stability-dependent SGS eddy viscosity and mixing length seems equally successful and computationally less expensive. The most widely used relation is

$$K = \ell^2 S(1 - \mathrm{Rf})^{1/2} \tag{13.54}$$

which may be considered a generalization of Equation (13.49). The additional influence of stability on the mixing length ℓ should also be considered so that the ratio ℓ/ℓ_o decreases with increasing stability. The ratio of SGS diffusivities of heat and momentum may also depend on Rf or Ri. Such a stability-dependent SGS model is considered to be crucial to the large-eddy simulation of the SBL.

Further refinements in SGS modeling have been proposed, especially for the satisfactory LES of the stratified surface layer. As the surface is approached, the relative contribution of subgrid motions to the total fluxes and TKE increases and must be accounted for by the SGS model. The simple Smagorinski model is found to be unsatisfactory and considerably overestimates the mean velocity gradients. The split-eddy viscosity model of Sullivan *et al.* (1994) appears to be quite promising (Andren, 1995), as more complex dynamic and stochastic subfilter models (Mason, 1994) require much larger computational resources. One may also consider using a TKE closure model in which the SGS eddy viscosity and the rate of energy dissipation are parameterized as

$$K = C\ell E^{1/2} \tag{13.55}$$

$$\varepsilon = C_\varepsilon E^{3/2}/\ell \tag{13.56}$$

Note that the estimated values of $C \cong 0.1$ and $C_\varepsilon \cong 0.93$ by Moeng and Wyngaard (1988) are quite different from the similar constants in the expressions (13.39) and (13.40) involving the total (overall) eddy viscosity and TKE. In the surface layer, ℓ is specified as an increasing function of height, such that $\ell = kz$ close to the surface and it approaches its constant value ℓ_o in the interior flow. The following interpolation formula is frequently used for this purpose:

$$\ell^{-n} = (kz)^{-n} + \ell_o^{-n} \tag{13.57}$$

in which an optimum value of $n \cong 2$ has been determined (Mason, 1994). A refinement of the vertical mesh near the surface, so that Δz is sufficiently small close to the surface and gradually increases to its constant interior value has also been recommended.

LES studies of the PBL The numerical solution of the grid-volume-averaged equations of motion, potential temperature, and scalar concentrations with an appropriate SGS model also depends on the initial and boundary conditions. In LES studies of the PBL, the initial conditions are usually specified assuming a simple reference state of the atmosphere in geostrophic balance, using actual sounding data, or results of an analytical model. The initial velocity profile may also contain small random fluctuations at all grid points. It is hoped that after

some spinup time, model results essentially become independent of the somewhat arbitrary initial conditions and depend only on the relevant external forcings, such as large-scale pressure gradients, the surface roughness, and the surface heat flux or temperature, that are also specified directly as surface and upper boundary conditions.

The LES approach has most successfully been utilized for studying the mean structure as well as turbulent transport and diffusion processes in unstable and convective boundary layers. Deardorff (1970a, 1972a) was the first to use this approach (he called it three-dimensional numerical modeling) for studying neutral and unstable atmospheric boundary layers with specified surface roughness, surface heat flux, and horizontal pressure gradients (representing a constant geostrophic wind). A rigid lid was imposed at the top of the model domain for a crude simulation of an inversion at the top of the mixed layer. Thus, only simple cases of barotropic, stationary, unstable and neutral PBLs with no entrainment from the top were simulated in this early study. Still, the results of numerical simulations led to an important discovery of mixed-layer similarity scaling by Deardorff (1970b). They also confirmed that the gradient-transport hypothesis is not generally valid in unstable and convective mixed layers in which large scale convective motions (updrafts and downdrafts) dominate turbulent transport and diffusion processes. The most remarkable of his LES results were the displays of the instaneous fields showing large-eddy structures and their evolution in time and space. Ensemble or horizontal spatial averages of simulated fields including turbulence statistics provided further justifications for utilizing the proposed similarity theories and scaling for neutral and convective boundary layers.

More realistic simulations of the evolving unstable and convective boundary layers were obtained by Deardorff (1974) by replacing the rigid lid at the top by an inversion layer, allowing for penetrative convection and entrainment of the free atmospheric air, and using more sophisticated higher-order SGS closure models. Increased computer power also permitted increased domain size and grid resolution in the model. Deardorff's (1974) LES results compared well with observations during convective conditions. They were also used in formulating better models of the evolution of the mixed-layer height and entrainment velocity. Later, Deardorff (1980) extended the LES approach to study stratocumulus-capped mixed layers. His pioneering LES studies at the National Center for Atmospheric Research were followed by other LES studies of turbulence and diffusion in the CBL (Moeng, 1984; Wyngaard and Brost, 1984; Moeng and Wyngaard, 1988; Nieuwstadt *et al.*, 1992).

An intercomparison of four different SGS parameterizations, by Nieuwstadt *et al.* (1992) shows that the simulated mean flow and turbulent structure of the convective mixed layer are not very sensitive to the details of SGS parameterization. However, the mean gradients and turbulence in the shear-dominated

surface layer are found to be strongly dependent on the SGS parameterization or model. In particular, the simple Smagorinski model has been shown to be inadequate and more sophisticated SGS models with better treatment of near-surface turbulent transfer processes are recommended for more realistic simulations of the surface layer of the CBL as well as other shear flows, such as neutral and stably stratified PBLs (Mason, 1994; Sullivan *et al.*, 1994).

Although the neutral PBL was included in Deardorff's (1970a, 1972a) early LES studies, more recent simulations of the same have revealed a much stronger sensitivity of results to the details of SGS parameterization and much slower approach to steady state or equilibrium condition than previously realized (Andren *et al.*, 1994). In particular, the mean fields (e.g., the velocity components U and V) show large inertial oscillations whose amplitudes decrease with increasing dimensionless time tf. But, it would take more than ten inertial periods ($tf > 10$) to reach a near steady state. The mean velocity gradients vary only slowly in time and higher moments (e.g., turbulent variances and fluxes) are less sensitive to the inertial oscillation. For example, the layer-averaged TKE reaches its equilibrium value only after one or two inertial periods.

In the intercomparison study by Andren *et al.* (1994), a shallow neutral PBL was simulated using four different LES models and a rather coarse grid so that results might be sensitive to the details of SGS parameterization or model. It is found that mean gradients and turbulence structure are indeed sensitive to the magnitude of the SGS eddy diffusivities. Resolved-scale motions are generally more intense in the lower part of the PBL in the models with smaller SGS eddy diffusivities. For the mean fields, the noted failure of the Smagorinski SGS model in producing the logarithmic mean wind and scalar profiles cannot be corrected by changing the value of the Smagorinski coefficient C_s. Differences between models with and without stochastic backscatter are, in general, largest close to the surface, but also noticeable in the lower one-third of the PBL. Sullivan *et al.* (1994) have proposed an alternative two-part eddy viscosity model for the shear-dominated lower (near-surface) layer. Their model utilized the TKE closure, but can be adopted in a first-order SGS closure model as well (Ding *et al.*, 2001a, b).

Although the LES approach has successfully been used for modeling neutral, unstable and convective boundary layers for more than thirty years, its application to the SBL started only recently when increased computer speed and memory permitted the use of a small enough grid size for most of the TKE to be resolved. Mason and Derbyshire (1990) used a modified version of the Smagorinski SGS model in which SGS eddy viscosity was related to flux Richardson number. They conducted a series of simulations of slightly stable boundary layers and showed their results to be broadly consistent with observations and the local similarity theory of Nieuwstadt (1984). Later Brown *et al.* (1994) used a revised version of Mason and Thomson's (1992)

stochastic backscatter model and extended the stability range to include moderately stable conditions (L = 31 m to 517 m and h/L = 1.4 to 5.4). The use of stochastic backscatter in their SGS model resulted in better resolution of turbulence and more realistic velocity and temperature profiles in the surface layer, which are consistent with the empirical Monin–Obukhov similarity functions. Their LES results are found to be quite sensitive to the SGS model with or without the stochastic backscatter.

The importance of using a good SGS model in the LES of the SBL has also been demonstrated by Andren (1995) who compared the results of simulations with two different SGS models, viz., Moeng's (1984) TKE closure model with a standard SGS mixing length formulation and that with a more refined two-part eddy viscosity formulation of Sullivan *et al.* (1994). Mean velocity and scalar gradients in the surface layer are much better simulated by the two-part eddy viscosity model which is found to be comparable to the computationally more expensive stochastic backscatter model of Brown *et al.* (1994). It yields more vigorous resolved-scale fields. The variance and covariance profiles in the simulated slightly stable boundary layer are well represented by their similarity forms (13.12)–(13.14). Eddy diffusivities of momentum, heat, and any passive scalar show similar distributions with normalized height in the SBL with their maximum values occurring around $z/h \cong 0.25$. Scalar diffusivities are 20–30% larger than eddy viscosity in the bulk of the SBL, but their ratios (K_h/K_m, etc.) decrease with sharply increasing Richardson number (Ri) near the top of the SBL.

Kosovic and Curry (2000) used a more complicated and computer intensive, nonlinear SGS model which is capable of reproducing the effects of backscatter of energy and of the SGS anisotropies that are characteristic of shear-driven flows. They explored the effects of the changes in surface cooling rate, geostrophic wind, inversion strength, surface roughness, and latitude on the mean flow and turbulence structure of the simulated SBL and carried out 21 LES cases with three different grid resolutions. The simulation times varied from 12 h to 24 h, depending on the latitude and corresponded to approximately six times the inertial period (f^{-1}). In order to test the SGS model effects, Kosovic and Curry (2000) also ran two simulations with the linear SGS models used by Andren (1995). A comparison of the normalized total (domain-averaged) TKE for different LES cases showed that the Smagorinski-type model is too dissipative, resulting in unrealistically low TKE levels. But, the linear two-part eddy viscosity model of Sullivan *et al.* (1994) produced much higher TKE levels which are 2–3 times larger than those produced by Kosovic's nonlinear model for the same grid resolution. The simulated TKE levels with the nonlinear SGS model also showed strong sensitivity to grid resolution. Longer simulation time resulted in the development of stronger inversion at the top of the SBL, which presented an obstacle to further SBL growth. But this

may be due to imposing a constant surface cooling rate, rather than the constant surface heat flux.

More recently, Ding *et al.* (2001a, b) have studied weakly unstable to moderately stable atmospheric boundary layers using the LES version of the Terminal Area Simulation System (TASS-LES) with a new SGS model. Their proposed SGS model incorporates some aspects of the two-part eddy viscosity model of Sullivan *et al.* (1994) and further refinements including the stability dependence of SGS mixing length and two-part separation of eddy diffusivity of heat similar to that of eddy viscosity. The strong sensitivity of the simulated mean velocity and potential temperature gradients in the lower parts of neutral and weakly unstable boundary layers to different SGS parameterizations or models is evident from Figure 13.9. The proposed two-part eddy viscosity and diffusivity model is found to be quite effective in simulating the empirical Monin–Obukhov similarity functions ϕ_m and ϕ_h in all the weakly unstable to moderately stable cases (see also Figure 13.10).

For their weakly unstable and neutral cases, Ding *et al.* (2001a) used a 2000 m × 2000 m × 750 m domain with 50 × 50 × 75 grid points in x, y, and z

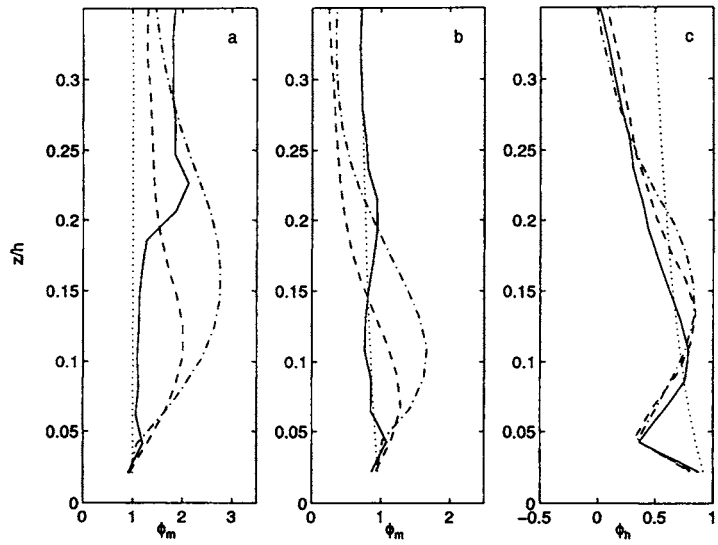

Figure 13.9 Comparison of simulated and empirical (measured) dimensionless gradients of mean velocity (a, b) and potential temperature (c) or Monin–Obukhov similarity functions in the lower part of the PBL for (a) the neutral case and (b) weakly unstable case. Dotted lines represent the empirical similarity functions, dashed-dotted lines the Smagorinski model, dashed lines the simplified two-part eddy viscosity model, and solid lines the proposed SGS model. [From Ding *et al.* (2001a).]

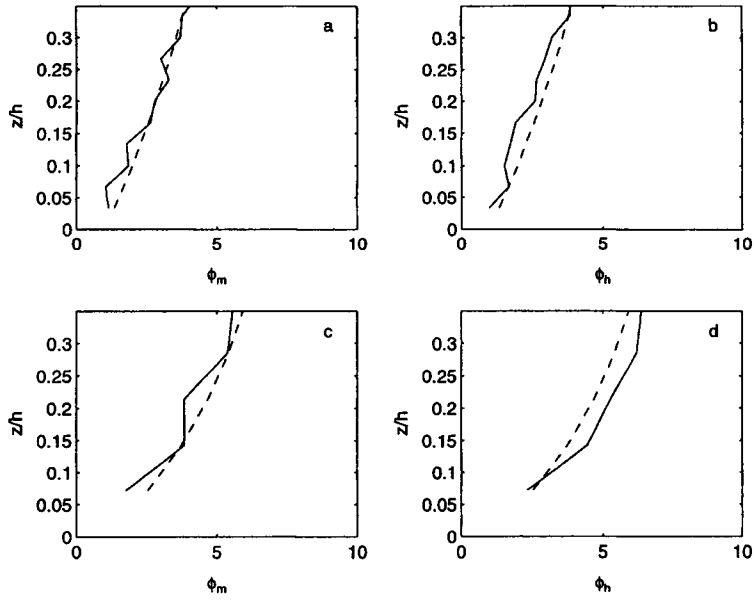

Figure 13.10 Comparison of simulated and empirical (measured) Monin–Obukhov similarity functions ϕ_m (a, c) and ϕ_h (b, d) in the lower part of the SBL. (a, c) The weakly stable WS1 case and (b, d) the moderately stable MS1 case. [From Ding *et al.* (2001b).]

directions, respectively. The initial potential temperature is 300 K below 450 m; it increases by 8 K across the 60 m thick inversion layer from 450 m to 510 m, and further increases with a small gradient of 0.003 K m^{-1} above 510 m. Initially, velocity field is in geostrophic balance with a constant geostrophic wind of 15 m s^{-1} in the x direction. The surface roughness parameter $z_0 = 0.16$ m and the surface heat flux is specified as 0.02 K m^{-1}. The simulation time for the weakly unstable case is 3.5 h of which the last 1 h is used for obtaining the average statistics. The simulation of the neutral case is built on the weakly unstable flow simulation by setting the surface heat flux to zero and running an additional 2 h simulation of which the last 1 h is used for obtaining averages. For these short simulation times, mean flow is not expected to attain a steady state, but turbulence structure reaches a quasi-steady state. Figure 13.11 shows the simulated momentum flux and TKE profiles for the neutral case. Note that the total momentum flux profile is close to linear with significant contributions from the proposed SGS model in the lower one-fourth of the PBL. The normalized TKE profile is characterized by large gradients in the surface layer with a maximum value of $\mathrm{TKE}/u_*^2 \cong 5.8$ near the surface. Although this value is consistent with observations of turbulence (velocity

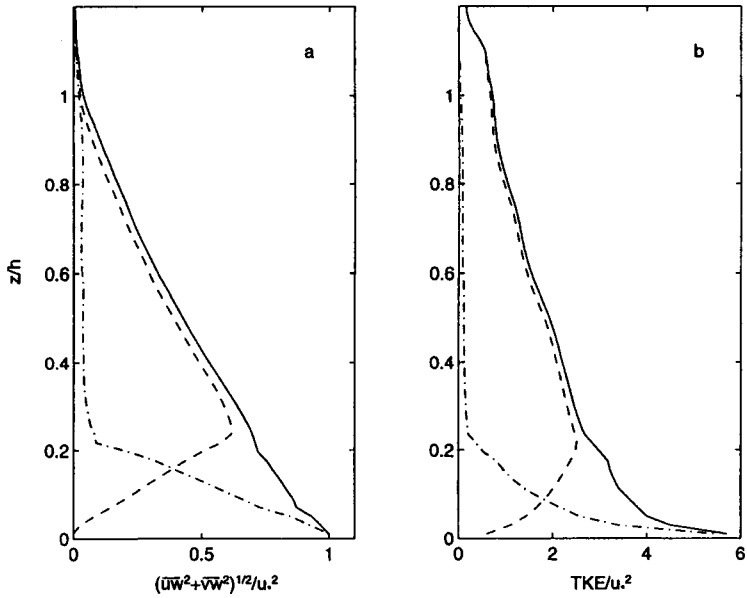

Figure 13.11 Ensemble-averaged profiles of the normalized (a) horizontal momentum flux and (b) TKE from the large-eddy simulation of the neutral PBL. Dashed lines represent resolved parts, dashed-dotted lines subgrid parts, and solid lines total flux and TKE. [From Ding *et al.* (2001a).]

variances and TKE) in the near-neutral surface layer, the rapid decrease of TKE with height is not consistent with the neutral surface-layer similarity theory.

The large-eddy simulations of weakly and moderately stable boundary layers by Ding *et al.* (2001b) are successively built from slightly unstable and neutral simulations by gradually reducing the surface heat flux in several steps. Most of the simulations had the same initial conditions but different geostrophic winds assuming a barotropic environment. Periodic boundary conditions are applied in horizontal (x and y) directions, while in the vertical direction, a sponge layer comprising of three grid intervals has been added on top of the model domain. Both the heat and momentum fluxes are assumed to vanish at the top boundary. The lower boundary employs a no-slip condition and the surface heat flux is specified as a function of time. Most simulations of the SBL are performed using small domains (e.g. 500 m × 500 m × 500 m) and finer grid resolutions (e.g. $\Delta x = \Delta y = \Delta z = 10$ m), although domain and grid sizes are also varied to examine their possible influences on LES results. Of the total simulation time of 6.5 h, a small positive (upward) surface heat flux is maintained during the first 1 h, followed by zero heat flux during the next 2 h, a decreasing negative heat flux during the next 2 h, and a constant negative (downward) heat flux in the

final 1.5 h of simulation. The final values of the specified surface heat flux ranged between -0.02 and $-0.05\,\mathrm{K\,m\,s^{-1}}$, while the specified geostrophic wind speed ranged between 7.5 and 15 $\mathrm{m\,s^{-1}}$. With different combinations of these external forcing parameters and an initial potential temperature profile with a 30 m thick inversion layer between 320 m and 350 m, several weakly and moderately stable cases could be simulated. Some of the LES results of a weakly stable (WS1) case and a moderately stable (MS1) case are presented here as illustrative examples.

Figure 13.12 compares the ensemble-averaged velocity and potential temperature profiles for the above two cases. These are similar to those typically observed in the SBL. In both cases, Θ profiles show a three-layer structure: a stable surface layer of strong gradients, a middle layer of small or vanishing gradients, and an elevated inversion layer on the top. However, in the moderately stable case, the lower layer has much stronger gradients, while the middle layer has almost zero gradient and is totally detached from the underlying shallow SBL. Wind speed profiles show the formation and evolution of the low-level jet whose height decreases and intensity increases with increasing time of simulation, especially in the weakly stable (WS1) case. A rather broad

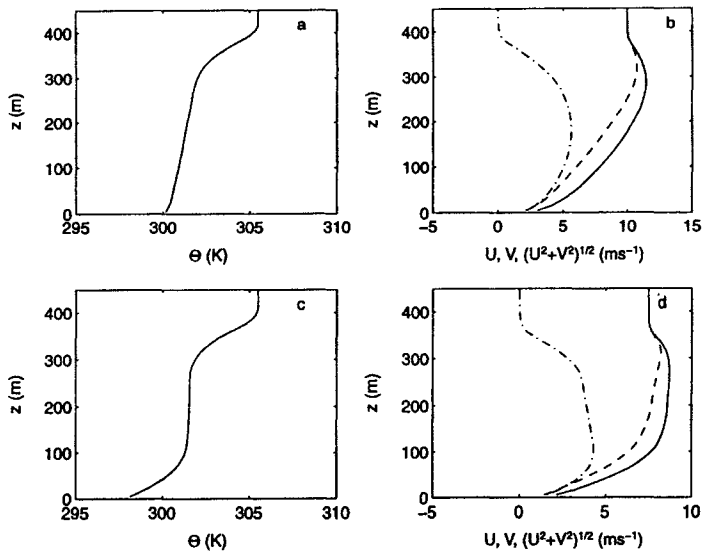

Figure 13.12 Ensemble-average profiles of (a) and (c) potential temperature, (b) and (d) wind speed, and horizontal velocity components in the simulated SBL. In (b) and (d) solid line represents wind speed, dashed line U-component, and dash-dotted line V-component. (a) and (b) the weakly stable (WS1) case; and (c) and (d) the moderately stable (MS1) case. [From Ding *et al.* (2001b).]

maximum in wind speed spans the entire depth of the residual layer in the moderately stable (MS1) case.

The simulated vertical distributions (profiles) of ensemble-averaged momentum flux, TKE, and heat flux are shown in Figures 13.13 and 13.14 for the two (WS1 and MS1) cases. They appear to be similar, except for the large difference in the SBL heights for the two cases. Both the momentum and heat fluxes decrease almost linearly with height in the lower part of SBL. The near-surface values of TKE/u_*^2 differ only slightly between weakly and moderately stable cases.

Much larger differences are found in the time histories (evolution) of TKE and Ri in weakly and moderately stable cases, as revealed by Figures 13.15 and 13.16. These figures show spatial distributions of instantaneous Ri and TKE in a horizontal plane in the middle of the SBL at four different times during the simulated evolution of the SBL: 200, 250, 300, and 350 minutes. Note that in the weakly stable case, TKE contours show large areas of continuous turbulence in which $\mathrm{Ri} < 0.25$. In the moderately stable case at $t = 350$ min, however, Ri values are greater than 0.25 in almost the entire domain and TKE contours reveal very weak and patchy turbulence. Figure 13.17 shows the time evolution of the domain-averaged TKE for the two cases. Note that, following the evening

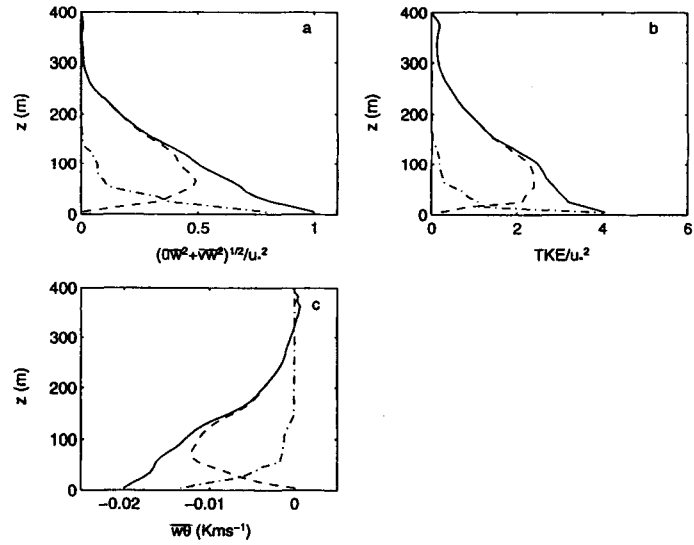

Figure 13.13 Ensemble-averaged profiles of (a) normalized momentum flux, (b) normalized TKE, and (c) heat flux from the simulation of the weakly stable case WS1. Dashed lines represent resolved parts, dash-dotted lines subgrid parts, and solid lines total fluxes and TKE. [From Ding *et al.* (2001b).]

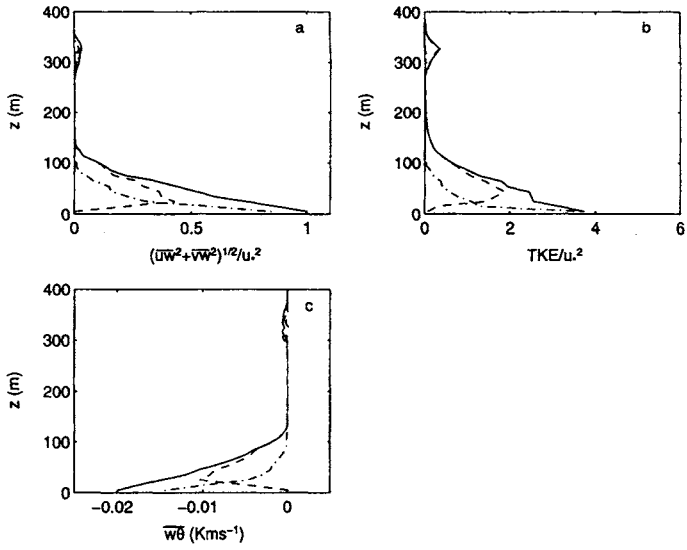

Figure 13.14 Same as Figure 13.13. but for the moderately stable case MS1. [From Ding *et al.* (2001b).]

transition period when the surface heat flux is zero, turbulence in the SBL decays in response to decreasing surface heat flux with time. A quasistationary state with nearly constant value of the domain-averaged TKE is reached only after 300 min when the surface heat flux is held constant.

13.4 Parameterization of the PBL

The governing equations of motion, thermodynamic energy, specific humidity, and other scalars used in large-scale models of the atmosphere contain subgrid scale variances and covariances (fluxes) of subgrid scale perturbations of velocity, temperature, specific humidity, etc. (Pielke, 1984). A perturbation is defined as the deviation of a variable from its grid-averaged value where averaging is implied over the grid volume ($\Delta x \Delta y \Delta z$) as well as over the finite time increment (Δt). The subgrid scale perturbation fluxes must be parameterized in terms of grid-averaged variables in order to form a closed set of equations for the latter. An accurate or satisfactory parameterization of subgrid scale fluxes is crucial to the satisfactory performance of any mesoscale or large-scale model, because the terms involving subgrid scale perturbations are usually of the same order or even larger than the corresponding terms involving grid volume-averaged resolved variables (Pielke, 1984).

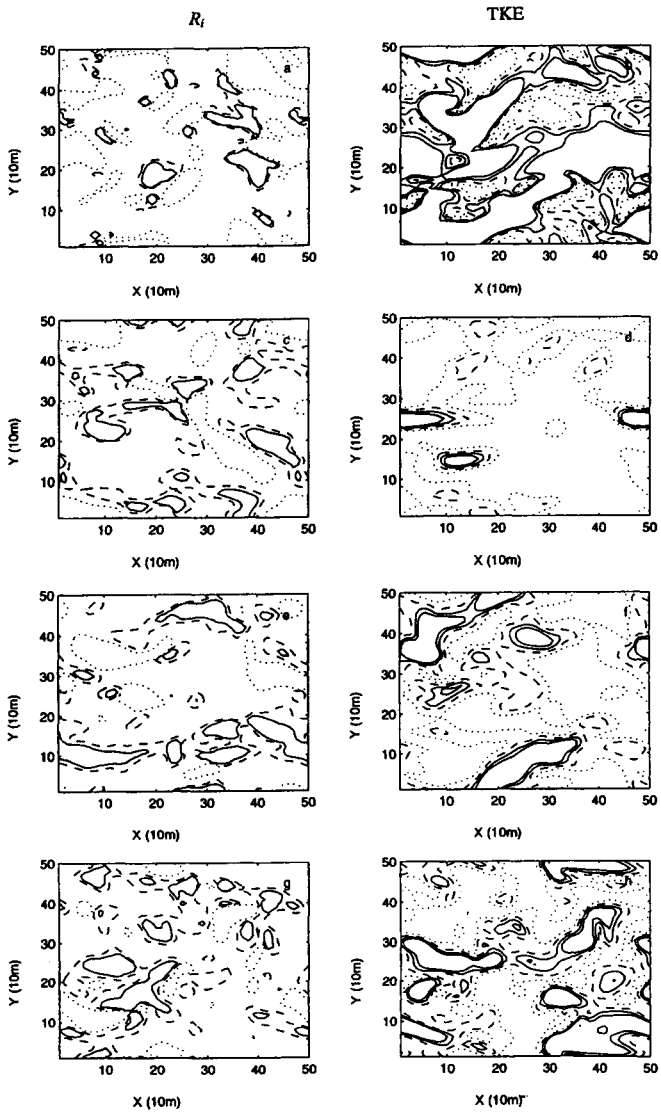

Figure 13.15 Spatial distribution of instantaneous R_i and TKE in a horizontal (x–y) plane near the middle of the SBL at four different times during the time evolution of the SBL in response to decreasing surface heat flux for the weakly stable case WS1: (a) and (b) $t = 200$ min.; (c) and (d) $t = 250$ min.; (e) and (f) $t = 300$ min.; (g) and (h) $t = 350$ min. (a), (c), (e) and (g) R_i contours: dotted lines represent 0, dashed lines 0.25, and solid lines 0.50; (b), (d), (f) and (h) TKE contours: dotted lines represent 0.05 $m^2\ s^{-2}$, dashed lines 0.10 $m^2\ s^{-2}$, and solid lines 0.15 $m^2\ s^{-2}$ or 0.20 $m^2\ s^{-2}$. [From Ding *et al.* (2001b).]

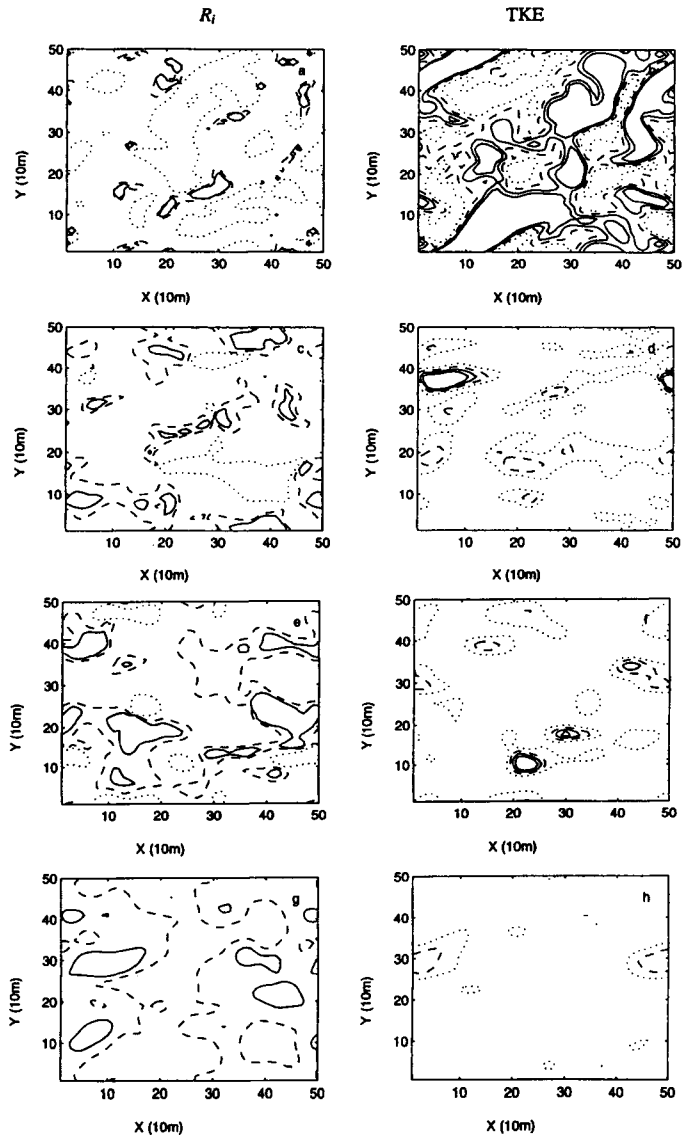

Figure 13.16 Same as Figure 13.15, but for the moderately stable case MS1. [From Ding *et al.* (2001b).]

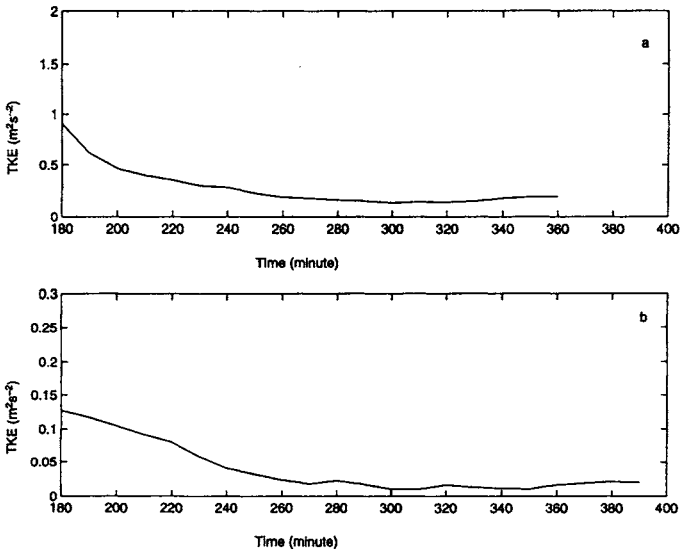

Figure 13.17 Time evolution of the domain-averaged TKE for (a) the weakly stable case WS1 and (b) the moderately stable case MS1 during the last 3.5 h simulation. [From Ding *et al.* (2001b).]

In developing parameterizations for subgrid-scale averaged quantities, it needs to be recognized that the preferred representation is an ensemble average over the grid volume rather than simply the grid volume average. The ensemble average represents the most likely value of the subgrid-scale quantity (variance or covariance) whereas the grid volume average represents just one realization (Pielke, 1984). Thus, most parameterizations discussed here may represent only the most likely (ensemble-averaged) estimates of subgrid-scale quantities. Another distinction that needs to be made, but is rarely recognized or even mentioned, is that between the subgrid-scale perturbation fluxes and the corresponding turbulent fluxes in the PBL. The former obviously depend on the grid spacings and may not be equal to the corresponding turbulent fluxes, except for the rare case when grid spacings are equal to the dimensions of the largest turbulent eddies. In large-domain mesoscale and large-scale models with horizontal grid sizes of tens or hundreds of kilometers, perturbation fluxes are likely to be larger than turbulent fluxes, because the former also contain the contributions of the subgrid mesoscale perturbations in addition to the contribution of turbulence. In mesoscale models of small domains with horizontal grid sizes of less than 2 km (i.e., the size of most energy-containing turbulent eddies), on the other hand, subgrid-scale perturbation fluxes might be smaller than the total turbulent fluxes. Since PBL parameterizations in

mesoscale models attempt to represent total ensemble-averaged fluxes due to turbulence only, these are most appropriate for mesoscale models with horizontal grid sizes of the order of 1 km.

13.4.1 Parameterization of turbulent fluxes

Most mesoscale atmospheric circulation and dispersion models attempt to resolve the PBL by placing several discrete grid levels within the lowest 1 km of the model domain. Ideally, the lowest grid level should lie within the surface layer. Anthes *et al.* (1980) have shown that a detailed multi-level resolution of the PBL is essential in a mesoscale model of flow over complex terrain with differential heating (e.g., across land–water boundaries), because significant vertical gradients of meteorological variables occur within the PBL. Simpler, mixed-layer representations of the PBL might be adequate in large-scale or general circulation models. Different types of parameterizations are used to represent the surface fluxes and turbulence variances, kinetic energy, fluxes, and scales at other discrete levels in the PBL, as these are usually not resolved by most widely used first-order closure models.

Surface fluxes The surface fluxes of momentum, heat, and moisture are usually parameterized by using the following bulk transfer relations:

$$\begin{aligned} \tau_0 &= \rho C_D V_1^2 \\ H_0 &= \rho c_p C_H V_1 (\Theta_0 - \Theta_1) \\ E_0 &= \rho C_E V_1 (Q_0 - Q_1) \end{aligned} \tag{13.58}$$

where V_1, Θ_1, and Q_1 are the mean wind speed, potential temperature, and specific humidity, respectively, at the first grid level (z_1), Θ_0 and Q_0 are the values at $z = z_0$, and C_D, C_H and C_E are the bulk transfer coefficients of momentum (C_D is also called the drag coefficient), heat and water vapor, respectively. Using a viscous or molecular sublayer parameterization, Θ_0 and Q_0 can be related to their values at the ground surface (Pielke, 1984).

In some large-scale models, using only crude parameterization of surface fluxes, constant values of bulk-transfer coefficients are specified with some distinction made between land and water surfaces and also between stable and unstable conditions. In most cases with large variations in surface roughness over the model domain and strong diurnal variations of stability in the surface layer, however, it is inappropriate to treat C_D and C_H (usually $C_E = C_H$) as constants. These could easily be specified as continuous functions of surface roughness and stability, using the Monin–Obukhov

similarity theory (Arya, 1984; Pielke, 1984). When z_1 lies in the surface layer, C_D and C_H can be represented as functions of z_1/z_0 and the bulk Richardson number

$$\mathrm{Ri_b} = \frac{g}{T_{v0}} \frac{(\Theta_{v1} - \Theta_{v0}) z_1}{V_1^2} \tag{13.59}$$

Computations show that C_D and C_H can vary over very wide ranges which depend on ranges of z_0 and $\mathrm{Ri_b}$ values encountered (Arya, 1977).

Fluxes and variances at interior levels Observations of heat and water vapor fluxes in unstable and convective boundary layers suggest that the fluxes vary more or less linearly from their maximum values at the surface to zero at the top of the PBL. For the total momentum flux, a linear profile is also expected under barotropic conditions. However, the presence of baroclinicity can cause large deviations from the linearity (Kaimal *et al.*, 1976). Observations in the SBL also suggest simple profiles of fluxes decreasing with height, as represented by Equations (13.12)–(13.14). The use of these similarity-scaled profiles of fluxes, variances and TKE should probably constitute the simplest parameterizations of these at interior levels in the PBL (Arya, 1984). The scaling parameters essentially depend on the surface fluxes, whose parameterization is discussed in the previous section, and the PBL height. These similarity-scaling-based parameterizations may not be applicable, however, in the vicinity of steep topographical features or sharp changes in surface characteristics.

A more widely used scheme for parameterizing the interior turbulent fluxes is based on the gradient-transport relations in which eddy diffusivities or mixing lengths are specified as functions of height and stability (Businger and Arya, 1974; Brost and Wyngaard, 1978; Pielke, 1984). An implicit specification of eddy diffusivities in terms of mixing lengths might be preferable to an explicit eddy diffusivity profile, especially in mesoscale models with fine vertical grid resolution in which vertical gradients are well resolved. The dependence of subgrid-scale mixing length on the vertical grid spacing can also be considered in such parameterizations.

In the above-mentioned gradient-transport scheme, fluxes are always down-gradient. Simple modifications to gradient-transport relations can also allow for some countergradient fluxes as often observed in the convective mixed layer (Deardorff, 1972a). More satisfactory parameterizations of subgrid-scale fluxes in the CBL would be those based on nonlocal mixing schemes, such as the asymmetric convective mixing (ACM) model (Pleim and Chang, 1992). These have already been discussed in Section 13.3.1.

13.4.2 Height of the PBL or inversion

In most of the parametric relations discussed here, the height of the PBL (h) or the capping inversion (z_i) is an important length scale which must be calculated or parameterized. A variety of theoretical models have been proposed in the literature for predicting h or z_i during the daytime unstable and convective conditions (Deardorff, 1974; Driedonks, 1982; Arya and Byun, 1987; Stull, 1988). Differences in the predictions of different types of models generally fall within the uncertainties of estimating the mean large-scale vertical velocity (W_h) at the top of the PBL.

The commonly used prognostic equation for the PBL height is Equation (13.29) in which both the entrainment velocity (w_e) and the mean vertical velocity (W_h) must be specified or parameterized. For example, the simple thermodynamic model of the mixed-layer growth described earlier in Equation (13.31) implies that

$$w_e = \frac{(1+C)}{\gamma h}\frac{H_0}{\rho c_p} \cong \frac{1.2}{\gamma h}\frac{H_0}{\rho c_p} \tag{13.60}$$

where $\gamma = \partial\Theta/\partial z$ just above the top of the mixed layer.

Deardorff (1974) has pointed out the various limitations of the above model and proposed the following interpolation expression based on his large-eddy simulations of the PBL:

$$w_e = \frac{1.8(W_*^3 + 1.1u_*^3 - 3.3u_*^2 fh)}{\gamma h^2(g/\Theta_0) + 9W_*^2 + 7.2u_*^2} \tag{13.61}$$

Note that in both Equations (13.60) and (13.61), the rate of growth of h is directly proportional to the surface heat flux and inversely proportional to the stability of the overlying inversion layer. Unlike Equation (13.60), Equation (13.61) remains well behaved and approximately valid during each of the limiting cases of vanishing γ, u_*, or W_*.

The evolution of the nocturnal stable boundary layer (SBL) is rather slow, except immediately following the evening transition period, and it is not clear whether a simple diagnostic relation of h, such as Equation (13.7), might be adequate or one should carry an appropriate rate equation for the same. Since the SBL constitutes only a shallow surface inversion layer of weak turbulent transports and small TKE, its detailed parameterization in a mesoscale or larger-scale model may not be that important.

Other aspects and details of the PBL parameterizations used in air pollution and dispersion applications have been described elsewhere (Arya, 1999, Chapter 4).

13.5 Applications

The material presented in this chapter describes the theories, models, and measurements of mean flow and turbulence in the homogeneous atmospheric boundary layer. It has practical applications in the following contexts or areas:

- boundary-layer meteorology;
- air pollution meteorology;
- similarity scales used for presenting the atmospheric boundary layer data in the dimensionless form;
- turbulence closure models of the PBL;
- large-eddy simulations of the PBL;
- mean wind and thermal structure of the PBL;
- parameterization of the PBL in large scale atmospheric models;
- parameterization of mean and turbulent transports and mixing height in atmospheric dispersion and air quality models.

Problems and Exercises

1. Compare and contrast between the daytime convective boundary layer and the nighttime stable boundary layer over a homogeneous land surface, considering the following PBL characteristics:
(a) mean potential temperature profile or thermal structure;
(b) mean wind speed and direction profiles;
(c) the PBL height and its evolution with time.

2.
(a) Distinguish between the mixed-layer similarity theory and scaling and the local free convection similarity theory and scaling. What are their limitations?
(b) Show that in the free convective surface layer, $\sigma_w/W_* = C_w(z/h)^{1/3}$, where C_w is an empirical constant.

3. The following observations were made at a suburban site during a summer afternoon:

Mean wind speed at 10 m height = 1.5 m s^{-1}.
Mean temperature at 10 m height = 27.0°C.
Sensible heat flux near the surface = 500 W m^{-2}.
Height of the inversion base = 2000 m.

Using the mixed-layer similarity relations, estimate the following:
(a) Deardorff's convective velocity;
(b) standard deviation of horizontal velocity fluctuations in the mixed layer;
(c) turbulence kinetic energy at 10, 100, 1000 m;
(d) the rate of energy dissipation at 100, 1000, and 2000 m.

4.
(a) Discuss the implied assumptions in the derivation of the SBL height relation (13.7), as well as its implications and possible limitations when $L/f \to \infty$.
(b) What are the other height scales that might limit the SBL height under slightly stable conditions and even moderately stable conditions in low latitudes?
(c) Compare the SBL height from Equation (13.7) with the neutral PBL height $h = cu_*/|f|$ and estimate the range of stability parameter μ_* in which the former is larger than the latter. Which of the two height expressions should be used under such slightly stable conditions and why?

5. Use the mean wind and temperature data from the Cabauw mast, given in Problem 3 of Chapter 6, and estimate the following scaling parameters using the appropriate similarity relations:
(a) u_* and L from the surface layer (5 m and 10 m) data;
(b) the SBL height from Equation (13.7);
(c) the heights where wind speed and Ri are maximum.
(d) Compare the different estimates of the SBL height with the measured value of 100 m by a colocated sodar, and comment on the accuracy or uncertainty of such estimates.

6. Discuss the relative merits and limitations of the Rossby number and generalized similarity theories of the PBL. Which one would you prefer for representing the turbulence structure (e.g. the vertical profiles of fluxes, variances, and TKE) of (a) the SBL and (b) the CBL and why?

7.
(a) Simplify the Equations (13.16) of mean motion for the stationary and horizontally homogeneous PBL and integrate them with respect to height z from zero to the top of the PBL to obtain the expressions for the momentum fluxes $(\overline{uw})_0$ and $(\overline{vw})_0$ at the surface.

(b) Show that, if the surface-layer coordinate system is used with the x axis oriented along the mean wind direction near the surface

$$\int_0^h (U - U_g)dz = 0$$

Discuss the implication of this integral constraint on the U profile under barotropic and baroclinic conditions with $\partial U_g/\partial z > 0$ and $\partial U_g/\partial z < 0$. Under what conditions would you expect a stronger low-level jet?

(c) Similarly, obtain the expressions for $\overline{uw}$ and $\overline{vw}$ at any height z and describe an indirect method of determining the stress profiles from the vertical sounding of mean winds and geostrophic winds.

8.

(a) What are the merits and limitations of the first-order local closure models of the PBL?

(b) Describe a simple nonlocal closure model that might be more appropriate for the convective boundary layer.

9.

(a) Using the simple thermodynamic integral model Equation (13.33), obtain an expression for the time evolution of the mixed-layer height for a sinusoidal variation of the surface heat flux with time during the daytime period P_d between sunrise and sunset.

(b) Using the above expression of the mixed-layer height with $P_d = 14h$ and $h_0 = 200$ m examine the sensitivity of the evolution of the mixed-layer height to $(\overline{w\theta})_{max}/\gamma$ within the expected range of this parameter (say, 10^4–10^6).

10.

(a) In the TKE closure relations (13.39)–(13.40) with parameterized length scales ℓ and ℓ_ε, show how you would estimate the two empirical constants from the well-known empirical similarity relations in the neutral surface layer.

(b) Are the same values of the constants also applicable to stratified surface layers and the PBL as a whole? Give reasons for your answer.

11.

(a) Discuss the uncertainties in the estimates of the empirical constants C_k, C_1 and C_2 that appear in the E–ε model equations. Are the so-called 'standard'

values of these constants, based on laboratory experiments, also applicable to the atmospheric boundary layer and why not?

(b) Discuss the limitations of the TKE closure models for their application to the ABL, especially under unstable and convective conditions.

12.

(a) Discuss the merits and limitations of second- and higher-order closure models.

(b) Compare and contrast the large-eddy simulation approach with higher-order closure modeling.

(c) Distinguish between the first-order subgrid-scale closure model and a similar ensemble-averaged closure model, and show that the former may not have the same limitations as the latter.

13. Of all the PBL and turbulence modeling approaches discussed in Chapters 9 and 13, which one would be the most appropriate to use and why, for the following situations:

(a) Evolution of the atmospheric boundary layers over a period of several days.

(b) Modeling the morning and evenings transitions between stable and unstable boundary layers and vice versa.

(c) Simulating the turbulence generation and decay processes is a very stable, shallow PBL.

(d) Modeling and parameterizing the turbulent exchange processes in the PBL in a mesoscale atmospheric model.